These proofs may contain colour figures. Those figures may print black and white in the final printed book if a colour print product has not been planned. The colour figures will appear in colour in all electronic versions of this book.

to similar features in the MSIS-predicted atmospheric profiles (Fig. 6.11A and B), which are found to be associated with disturbed conditions due to geomagnetic activities. It is unclear whether this is physically meaningful or due to some problem with the empirical model of MSIS-90 in accounting for atmospheric responses during extreme geomagnetic events, which, nevertheless, does not affect our discussions. The high degree of variability as illustrated in Fig. 6.11 clearly underscores the necessity and importance of implementing self-consistent particle-impact ionization calculation within any global models, which are facilitated by the availability of the accurate and computationally efficient parameterization models. It should be pointed out that none of the empirical ionization formulae that have been reviewed in this section can be directly extended to nonterrestrial atmospheres, considering that different atmospheric compositions would lead to different interaction processes between charged particles and atmospheric neutrals and thus different collisional effects.

s0150 6.3 Electromagnetic fields of magnetospheric disturbances in the conjugate ionospheres: Current/voltage dichotomy

Vyacheslav A. Pilipenko[a, b], Mark J. Engebretson[c], Michael D. Hartinger[d], Evgeny N. Fedorov[b] and Shane Coyle[d]

[a]Space Research Institute, Moscow, Russia

[b]Institute of Physics of the Earth, Moscow, Russia

[c]Augsburg University, Minneapolis, MN, United States

[d]Virginia Tech, Blacksburg, VA, United States

s0155 6.3.1 Introduction: Current/voltage dichotomy

p0885 When considering a circuit analogy of the magnetosphere-ionosphere current systems it is physically intuitive to distinguish between generators which deliver a fixed current, and those in which the voltage is fixed (Lysak, 1985). This qualitative consideration may be visualized as a magnetospheric generator with an internal resistance and an ionospheric load. If the internal resistance is small compared to the load on the circuit, the ionosphere will receive a fixed voltage, whereas if the load is small compared to the internal resistance, a fixed current will be delivered to the ionosphere (Lysak, 1990).

p0890 Magnetosphere-ionosphere transient current systems with typical timescales in the lowest-frequency portion of the ULF band (1–15 min) are also often described using this electrical circuit analogy (Hartinger et al., 2017). A magnetospheric process can generate a potential difference that maps along magnetic field lines to the ionosphere, where it drives electric fields. On the other hand, magnetospheric processes can generate divergent currents perpendicular to the background magnetic field which in the ionosphere are closed via field-aligned currents (FACs). In the case of a current generator, the

To protect the rights of the author(s) and publisher we inform you that this PDF is an uncorrected proof for internal business use only by the author(s), editor(s), reviewer(s), Elsevier and typesetter SPi. It is not allowed to publish this proof online or in print. This proof copy is the copyright property of the publisher and is confidential until formal publication.

These proofs may contain colour figures. Those figures may print black and white in the final printed book if a colour print product has not been planned. The colour figures will appear in colour in all electronic versions of this book.

magnetic effect on the ground must be nearly the same under sunlit or dark ionospheres, whereas in the case of a voltage generator the ground magnetic response must be much larger under a highly conductive ionosphere (Sibeck et al., 1996; Lam and Rodger, 2004). The dependence of the ULF response to magnetospheric driving on the ionospheric conductance may be an important observational feature of a coupled magnetosphere-ionosphere system. An adequate incorporation of the interhemispheric differences and their effects on magnetosphere-ionosphere coupling is vitally important for observations and modeling/simulations (Zesta et al., 2016).

p0895 There are several possibilities to examine the dependence of ground magnetic response to a magnetospheric driver on the ionospheric conductance. The first one is to study the daily variations of magnetic disturbance amplitude at a selected station. However, the intensity of a magnetospheric driver may vary from hour to hour. The second is to examine the seasonal variation of the disturbance amplitude. Upon examining the seasonal variations, for a magnetospheric FAC generator the local ionospheric resistance plays the role of a load resistance, whereas the Alfvén wave resistance and the resistance of conjugate ionospheres play the role of an internal source resistance (Pilipenko et al., 2019). Such a combination of several poorly known parameters makes an unambiguous interpretation of seasonal variations difficult. Finally, the current/voltage paradigm can be tested in a straightforward way with observations at conjugate stations under strongly asymmetric ionospheres.

p0900 An important aspect of the ULF magnetospheric disturbance interaction with the ionosphere which should be taken into account when considering the current/voltage dichotomy is that FACs may interact with the ionosphere in a different way in regimes of forced driving or excitation of resonant field line oscillations (Pilipenko et al., 2019). Here, we compare the results of observations of various ULF phenomena, such as TCVs, Pc5 waves, SCs, and MPEs at conjugate magnetometer arrays in Greenland and Antarctica from the viewpoint of the voltage/current generator dichotomy. But first, theoretical predictions of a simple "plasma box" model of the magnetosphere with asymmetric conjugate ionospheres driven by magnetospheric FAC are summarized.

s0160 6.3.2 Model of a magnetosphere with asymmetric ionospheres

p0905 The "plasma box" model of the magnetosphere (Fig. 6.12) mimics the magnetosphere at middle and high latitudes. Magnetospheric straight field lines with length $2L$ are terminated by thin ionospheric layers with height-integrated Pedersen and Hall conductances Σ_P and Σ_H, respectively. The coordinate x corresponds to the Earthward radial direction, the z-axis is along the geomagnetic field $\mathbf{B}_0$, and the y-axis corresponds to the azimuthal direction (the system is homogeneous in this direction).

p0910 Let at some magnetic shell a transient pulse of FAC $j_z(t)$ be excited by an external transverse current $j_x^{(e)}$. The radial direction of an external current corresponds to an

To protect the rights of the author(s) and publisher we inform you that this PDF is an uncorrected proof for internal business use only by the author(s), editor(s), reviewer(s), Elsevier and typesetter SPi. It is not allowed to publish this proof online or in print. This proof copy is the copyright property of the publisher and is confidential until formal publication.

These proofs may contain colour figures. Those figures may print black and white in the final printed book if a colour print product has not been planned. The colour figures will appear in colour in all electronic versions of this book.

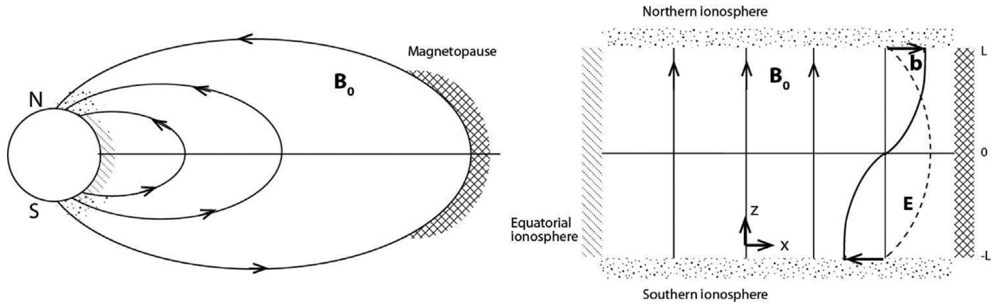

f0065 **Fig. 6.12** Field-aligned currents excitation in a simple "magnetospheric box" model: homogeneous plasma with constant Alfvén velocity V_A immersed in a straight magnetic field B_o. The field lines with length $2l$ are terminated by conjugate dayside Southern (S) and Northern (N) ionospheres with conductances $\Sigma_P^{(S)}$ and $\Sigma_P^{(N)}$. The oscillations are driven by an external transverse current $j_x^{(d)}$.

azimuthally (along the Y-axis) large-scale disturbance. The electric field of the disturbance $\mathbf{E}_\perp = (E_x, E_y)$ is described by the MHD wave equation

$$\left(\partial_z^2 - V_A^{-2}\partial_t^2\right)E_x(t,z) = \mu_0 \partial_t j_x^{(e)}(t,z) \tag{6.57}$$

The magnetic component of a disturbance can be found from Maxwell's equations as $\partial_t B_y = -\partial_z E_x$. Eq. (6.57) describes an Alfvénic-type disturbance carrying a nonsteady FAC $j_z = \Sigma_A \nabla E_\perp$, where $\Sigma_A = (\mu_o V_A)^{-1}$ is the magnetospheric Alfvén conductance determined by the Alfvén velocity V_A. The fundamental Alfvén wave period in the magnetospheric box model is $T_A = 4L/V_A$.

p0915 Eq. (6.57) should be augmented by the impedance-type boundary conditions at conjugate Northern (N) and Southern (S) ionospheres ($z = \mp L$) as follows (Newton et al., 1978):

$$B_y = \mp \mu_0 \Sigma_P E_x \tag{6.58}$$

Let the driving current be localized at the magnetospheric equatorial plane ($z=0$), namely, $j_x^{(e)}(z) = J_e(t)\delta(z)$. Integrating Maxwell's equations across the area occupied by a driver, the conditions on a jump of transverse magnetic and electric fields can be obtained

$$\{E_x\}|_{z=0} = 0, \quad \{B_y\}|_{z=0} = -\mu_0 J_e(t) \tag{6.59}$$

where $\{\ldots\}$ denote a jump across the source region. The interaction of an Alfvén wave with the ionosphere is characterized by the reflection coefficient

$$R^{(S,N)} = \frac{\overline{\Sigma}_P^{(S,N)} - 1}{\overline{\Sigma}_P^{(S,N)} + 1} \tag{6.60}$$

determined by the ratio between the ionospheric Pedersen conductance and wave conductance, $\overline{\Sigma}_P^{(S,N)} = \Sigma_P^{(S,N)}/\Sigma_A$.

To protect the rights of the author(s) and publisher we inform you that this PDF is an uncorrected proof for internal business use only by the author(s), editor(s), reviewer(s), Elsevier and typesetter SPi. It is not allowed to publish this proof online or in print. This proof copy is the copyright property of the publisher and is confidential until formal publication.

These proofs may contain colour figures. Those figures may print black and white in the final printed book if a colour print product has not been planned. The colour figures will appear in colour in all electronic versions of this book.

p0920 Steady-state solutions above the ionospheres for $E_x(z) = ik\varphi$ and $B_y(z) = -ik\psi$ can be obtained via the electric and magnetic potentials

$$\begin{aligned} \varphi^{(S,N)}(z) &= \mp V_A \left[\exp\{\mp ik_A(z \pm L)\} - R^{(S,N)} \exp\{\pm ik_A(z \pm L)\} \right] \\ \psi_{S,N}(z) &= \exp\{\mp ik_A(z \pm L)\} + R^{(S,N)} \exp\{\pm ik_A(z \pm L)\} \end{aligned} \tag{6.61}$$

Here, the upper/lower signs correspond to S/N hemispheres, and $k_A = \omega/V_A$ is the Alfvén wave number. These solutions satisfy the boundary conditions at the ionosphere (6.58) and describe the field-aligned structure of a disturbance. The field-aligned distribution of electromagnetic field above and below the source of disturbances is found with account for the merging condition (6.59). Then, the ratio between electric $E^{(N)}/E^{(S)} = E_x(L)/E_x(-L)$ and magnetic $B^{(N)}/B^{(S)} = B_y(L)/B_y(-L)$ fields in the conjugate ionospheres can be derived as follows:

$$\frac{E^{(N)}}{E^{(S)}} = \frac{1 - i\overline{\Sigma}_P^S \tan(k_A L)}{1 - i\overline{\Sigma}_P^N \tan(k_A L)} \tag{6.62}$$

$$\frac{B^{(N)}}{B^{(S)}} = -\frac{\overline{\Sigma}_P^N}{\overline{\Sigma}_P^S} \frac{1 - i\overline{\Sigma}_P^S \tan(k_A L)}{1 - i\overline{\Sigma}_P^N \tan(k_A L)} \tag{6.63}$$

The magnetic B_x disturbance on the ground is related to an azimuthal magnetic disturbance B_y above the ionosphere by the well-known formula (Hughes and Southwood, 1976; Alperovich and Fedorov, 2007)

$$B_x^{(S,N)} = B_y^{(S,N)} \frac{\Sigma_H^{(S,N)}}{\Sigma_P^{(S,N)}} \exp(-kh) \tag{6.64}$$

where h is the height of the ionospheric conductive sheet and k is the horizontal wave vector of the disturbance. The ratio between the ground magnetic responses at the conjugate points is

$$\frac{B_x^{(N)}}{B_x^{(S)}} = \frac{B^{(N)}}{B^{(S)}} \frac{\Sigma_H^{(N)}}{\Sigma_P^{(N)}} \frac{\Sigma_P^{(S)}}{\Sigma_H^{(S)}} \tag{6.65}$$

Different situations are possible, as follows from these relationships (6.62 and 6.65), depending on the timescale of the disturbance τ and the local field-line resonant period T_A.

To protect the rights of the author(s) and publisher we inform you that this PDF is an uncorrected proof for internal business use only by the author(s), editor(s), reviewer(s), Elsevier and typesetter SPi. It is not allowed to publish this proof online or in print. This proof copy is the copyright property of the publisher and is confidential until formal publication.

These proofs may contain colour figures. Those figures may print black and white in the final printed book if a colour print product has not been planned. The colour figures will appear in colour in all electronic versions of this book.

s0165 #### 6.3.2.1 Relationship between ground magnetic disturbances at conjugate sites

p0925 In the case of nonresonant quasi-DC forced driving, when $\omega \ll \Omega_A$ (or $k_A L \ll 1$), from Eqs. (6.62), (6.65), the ratio between ground magnetic disturbances at conjugate points follows:

$$\frac{B_x^{(N)}}{B_x^{(S)}} = \frac{\overline{\Sigma}_H^{(N)}}{\overline{\Sigma}_H^{(S)}} \tag{6.66}$$

Thus, upon a quasi-DC driving the magnetic response must be larger under a higher local ionospheric conductivity, which corresponds to a voltage generator regime.

p0930 In the case of resonant driving, when the frequency of an oscillatory driver matches the local field line frequency of a magnetic shell, $\omega \to \Omega_A$ (or $k_A L = \pi/2$), the ratio of magnetic responses at conjugate points can be obtained from Eqs. (6.62), (6.65)

$$\frac{B_x^{(N)}}{B_x^{(S)}} \simeq \frac{\overline{\Sigma}_H^{(N)}}{\overline{\Sigma}_P^{(N)}} \frac{\overline{\Sigma}_P^{(S)}}{\overline{\Sigma}_H^{(S)}} \tag{6.67}$$

The ratio of ground magnetic responses at conjugate points does not depend on variations of the ionospheric conductance, which corresponds to the current generator regime. The change from voltage to current generator regime upon transfer from nonresonant to resonant driving is similar to the antireflective coating in optics, where the input impedance of a multilayered system changes dramatically when the wavelength of incident light is a multiple of the layer width.

s0170 #### 6.3.2.2 Field-aligned magnetosphere-ionosphere currents

p0935 The relationship between the FACs flowing into conjugate ionospheres $j_z \equiv j_\parallel$ and a driver current J_e can be found using Ampere's law $j_z = \mu_0^{-1} ikB_y$ as follows $j_\parallel^{(N)}/j_\parallel^{(S)} = B^{(N)}/B^{(S)}$. In the case of nonresonant quasi-DC driving, the FAC ratio is

$$\frac{j_\parallel^{(N)}}{j_\parallel^{(S)}} = -\frac{\Sigma_P^{(N)}}{\Sigma_P^{(S)}} \tag{6.68}$$

This relationship predicts that a larger FAC flows into a more-conductive ionosphere. In the regime of resonant driving, the magnitudes of FACs above the conjugate ionospheres are the same, namely

$$j_\parallel^{(N)} = -j_\parallel^{(S)} = kJ_e \frac{\overline{\Sigma}_P^{(N)} \overline{\Sigma}_P^{(S)}}{\overline{\Sigma}_P^{(S)} + \overline{\Sigma}_P^{(N)}} \tag{6.69}$$

To protect the rights of the author(s) and publisher we inform you that this PDF is an uncorrected proof for internal business use only by the author(s), editor(s), reviewer(s), Elsevier and typesetter SPi. It is not allowed to publish this proof online or in print. This proof copy is the copyright property of the publisher and is confidential until formal publication.

These proofs may contain colour figures. Those figures may print black and white in the final printed book if a colour print product has not been planned. The colour figures will appear in colour in all electronic versions of this book.

In the case of strongly asymmetric ionospheres, for example, $\overline{\Sigma}_P^{(N)} \gg \overline{\Sigma}_P^{(S)}$, from the above relationships it follows that FACs into both ionospheres are proportional to Pedersen conductivity of the less-conductive hemisphere, $j_\parallel^{(N)} = j_\parallel^{(S)} \propto \overline{\Sigma}_P^{(S)}$.

s0175 #### 6.3.2.3 Ionospheric electric fields in conjugate ionospheres

p0940 HF radar sounding of the ionosphere provides the possibility to monitor the ionospheric Doppler plasma velocities and consequently the electric field. The dense array of SuperDARN radars in both Northern and Southern hemispheres makes it possible to measure the ionospheric electric field response in conjugate ionospheres. The relevant magnitudes of electric fields in conjugate ionospheres are shown to be as follows.

p0945 In two limiting cases of quasi-DC forced driving and resonant excitation of Alfvén eigenoscillations, we arrive from Eq. (6.62) at the following ratios between electric disturbances at conjugate ionospheres:

$$\frac{E_N}{E_S} \simeq 1 \quad \text{when } \tau \gg T_A, \qquad \frac{E_N}{E_S} \simeq \frac{\overline{\Sigma}_P^{(S)}}{\overline{\Sigma}_P^{(N)}} \quad \text{when } \tau \simeq T_A \tag{6.70}$$

These relationships may be verified by comparing the amplitudes of ionospheric electric field disturbances detected simultaneously by SuperDARN radars in the Northern and Southern hemispheres.

s0180 ### 6.3.3 Spatial structure of resonant ULF waves and ionospheric conductivity

p0950 In the previous consideration, it has been assumed that a disturbance generated in the magnetosphere is a localized stream of FACs. However, the resonant ULF waves, such as Pc4–5 waves, are in fact a coupled MHD mode. So, upon interhemispheric comparison, their latitudinal structure should be taken into account. MHD disturbances from remote parts of the magnetosphere propagate inside the magnetosphere and, through a mode transformation, excite standing Alfvén oscillations. The process of the mode transformation is most effective in the vicinity of the resonant shells, where the local eigenfrequency $f_A(x)$ of Alfvén field line oscillations coincides with the frequency f of an external source (Chen and Hasegawa, 1974). The mathematical description of the spatial structure of the field perturbation in the magnetosphere can be expressed in the form of asymptotic expansion in the vicinity of a resonant field line (Kivelson and Southwood, 1986). The expansion of the azimuthal magnetic component $B_y(x, f)$ has a singularity at a resonant shell ($x \to x_A(f)$). At the same time, the radial $B_x(x, f)$ component has just a weak logarithmic singularity near the resonance, so the resonant behavior of this component would hardly be noticeable. The spectral MHD theory (e.g., Krylov et al., 1979) states that the resonant frequency and field-aligned structure of the coupled MHD mode

Q5 Q6

To protect the rights of the author(s) and publisher we inform you that this PDF is an uncorrected proof for internal business use only by the author(s), editor(s), reviewer(s), Elsevier and typesetter SPi. It is not allowed to publish this proof online or in print. This proof copy is the copyright property of the publisher and is confidential until formal publication.

These proofs may contain colour figures. Those figures may print black and white in the final printed book if a colour print product has not been planned. The colour figures will appear in colour in all electronic versions of this book.

are described by ordinary differential 1D equations, identical to equations for the uncoupled Alfvén modes in a homogeneous plasma (e.g., plasma box model).

p0955 Upon transmission through the ionosphere, the horizontal structure of ULF waves is distorted. This distortion can be analytically described for the Alfvén wave with a resonant Lorentz-type spatial structure transmitting through the "thin" ionospheric layer above an infinitely conducting ground (Hughes and Southwood, 1976; Alperovich and Fedorov, 2007): (a) the $\pi/2$ rotation of the wave polarization ellipse takes place, $B_y^{(m)} \rightarrow B_x^{(g)}$ (superscripts m and g denote field above the ionosphere and on the ground); (b) the width δ_g of the resonance peak, as observed at the ground, is wider as compared with the width δ_m above the ionosphere, $\delta_g = \delta_m + h$. The leading term which describes the amplitude of the north-south ULF wave component at the ground $B_x^{(g)}$ in the vicinity of a resonant magnetic shell can be written as

$$|B_x^{(g)}(x,f)| = B_o(f)\frac{\delta_m}{\sqrt{[x - x_A(f)]^2 + \delta_g^2}} \tag{6.71}$$

According to Eq. (6.71), the latitudinal structure of the ULF field can be qualitatively represented as the combination of a "source" spectrum $B_o(f)$ and a magnetospheric Alfvénic resonance response. The "source" part is related to a disturbance transported by a large-scale fast compressional wave and has a weak dependence on the x coordinate. The resonant magnetospheric response related to the Alfvén waves excitation is strongly localized and it causes rapid enhancement of amplitude at a resonant shell. The Alfvénic part is dominant in the vicinity of the resonant peak, $|x - x_A(f)| \leq \delta_g$. The width δ_g is determined by the dominant damping mechanism (Yumoto et al., 1995). One of the main damping mechanisms is ionospheric Joule dissipation (Newton et al., 1978). In order to drive a resonant system to the saturation level, a driver must be applied continuously during a time period of $\sim T_A Q$ (where Q is the quality factor of the resonant system). A realistic value for the dayside Alfvénic resonator in the Pc5 band is $Q \simeq 5-10$.

s0185 6.3.4 Alfvénic pulse incident on conjugate ionospheres

p0960 The transient Alfvénic response of the high-latitude magnetosphere to an interplanetary shock is a short impulse with duration τ much less than the Alfvén wave eigenperiod T_A of a field line, $\tau \ll T_A$. In this case, after excitation Alfvénic pulses propagate independently without attenuation toward Northern and Southern hemispheres away from the magnetospheric equatorial plane. At $t < T_A/4$, only incident (i) pulses can be seen in both hemispheres above the ionospheres. In this case, they are described as follows:

$$E_x^{(i)}(t,z) = \frac{1}{2\Sigma_A}\begin{cases} J_e(t + z/V_A) & \text{at } z < 0 \\ J_e(t - z/V_A) & \text{at } z > 0 \end{cases} \tag{6.72}$$

To protect the rights of the author(s) and publisher we inform you that this PDF is an uncorrected proof for internal business use only by the author(s), editor(s), reviewer(s), Elsevier and typesetter SPi. It is not allowed to publish this proof online or in print. This proof copy is the copyright property of the publisher and is confidential until formal publication.

These proofs may contain colour figures. Those figures may print black and white in the final printed book if a colour print product has not been planned. The colour figures will appear in colour in all electronic versions of this book.

p9900 The Alfvénic pulses reflected from the ionospheres (r) can be presented as

$$E_x^{(r)}(t,z) \ = -\frac{1}{2\Sigma_A}\left[R^{(S)}J_e\left(t-\frac{z+2L}{V_A}\right)+R^{(N)}J_e\left(t+\frac{z-2L}{V_A}\right)\right] \tag{6.73}$$

The total field structure around the ionosphere ($z \simeq \pm L$) is formed by incident (6.72) and reflected (6.73) pulses. The magnetic disturbance B_x on the Earth's surface produced by the Hall current induced by the impulse total field in the ionosphere $J_y = -\Sigma_H E_x$ is

$$B_x = -\mu_0 \frac{\overline{\Sigma}_H}{\overline{\Sigma}_P + 1} J_e(t - L/V_A) \tag{6.74}$$

In respect to the magnitude of the ionospheric conductance, the dependence of the ground response changes from a voltage generator regime ($\overline{\Sigma}_P \ll 1$) to a current regime ($\overline{\Sigma}_P \gg 1$). The ground magnetic response in the Northern and Southern hemispheres from Eq. (6.74) is as follows:

$$\frac{B_x^{(N)}}{B_x^{(S)}} = \frac{\overline{\Sigma}_H^{(N)}}{\overline{\Sigma}_H^{(S)}} \frac{\overline{\Sigma}_P^{(S)}+1}{\overline{\Sigma}_P^{(N)}+1} \tag{6.75}$$

In general, this relationship does not correspond directly to either the current or voltage regimes.

s0190 6.3.5 Resolving the current-voltage dualism with conjugate observations

p0965 The theoretical model predicts that upon the excitation of FAC in the magnetospheric resonator the dependence on the ionospheric conductance may look like a voltage or current generator, depending on the parameters of a magnetospheric disturbance, in particular on timescale of the driver regime τ and the local eigenperiod of the magnetospheric resonator T_A (Pilipenko et al., 2019). Here, we compare the results of various types of ULF disturbances at conjugate sites in the Arctic and Antarctic.

s0195 *6.3.5.1 Database and models*

p0970 We use data from the conjugate Antarctica-Greenland magnetometer arrays. Virginia Tech (http://mist.nianet.org) deployed an autonomous adaptive low-power instrument platform (AAL-PIP) network with sampling cadence 1 s in Antarctica. These sites are designed to be magnetically conjugate to the Greenland West Coast magnetometer chain along the $\Lambda \simeq 40$degrees magnetic meridian operated by the Technical University of Denmark (https://www.space.dtu.dk). Fig. 6.13 shows the locations of the AAL-PIP stations and the geomagnetic conjugate points of their counterparts in Greenland: PG0-UPN, PG1-UMQ, PG2-GDH, PG3-ATU, PG4-SKT, and PG5-GHB. Conjugate pair coordinates are given in Table 6.1. All stations are equipped with three-axes

To protect the rights of the author(s) and publisher we inform you that this PDF is an uncorrected proof for internal business use only by the author(s), editor(s), reviewer(s), Elsevier and typesetter SPi. It is not allowed to publish this proof online or in print. This proof copy is the copyright property of the publisher and is confidential until formal publication.

These proofs may contain colour figures. Those figures may print black and white in the final printed book if a colour print product has not been planned. The colour figures will appear in colour in all electronic versions of this book.

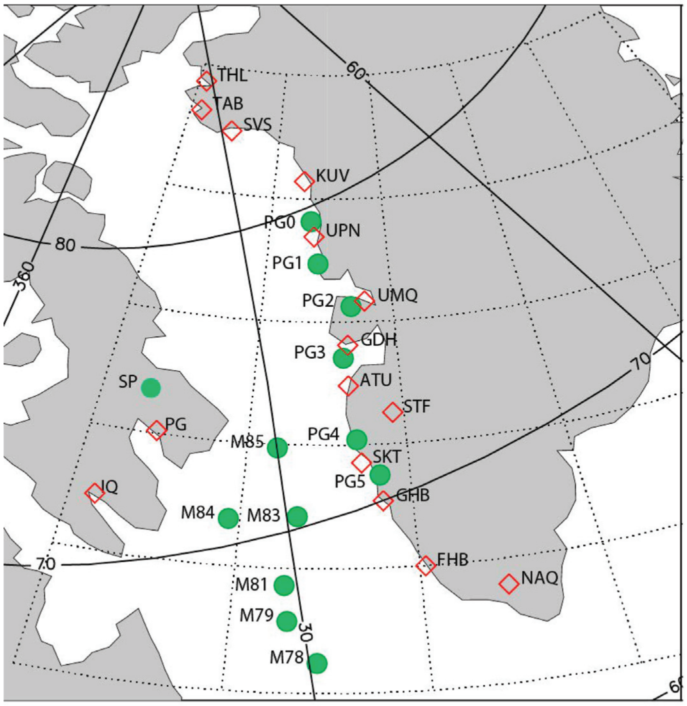

f0070 **Fig. 6.13** Map of Arctic Canada and Greenland, showing stations in the Northern hemisphere (*diamonds*) and the conjugate mapped locations of Southern hemisphere stations (*green circles*). *Solid lines* show corrected geomagnetic coordinates.

fluxgate magnetometers. The sensor axes are oriented along local magnetic north (B_x), local magnetic east (B_y), and vertically down (B_z). The AAL-PIP profile is augmented by the latitudinal profile of automated low-powered British Antarctic Survey (BAS) stations.

p0975 Because of the lack of direct information about the ionospheric conductivities, one has to use information from empirical models. Here, the height-integrated (80–1000 km) ionospheric conductivities have been estimated using the online resource of the Kyoto University (http://wdc.kugi.kyoto-u.ac.jp/ionocond/sigcal), based on the IRI-2016 model (Bilitza et al., 2017). The difference in ionospheric conductances in opposite hemispheres is controlled not only by the difference in solar illumination, but also auroral electron precipitation as well. A source of information on the auroral precipitation is the OVATION-prime (OP) model driven by solar wind and IMF parameters (http://sourceforge.net/projects/ovation-prime/). The OP model is based on energetic particle measurements from the Defense Meteorological Satellite Program (DMSP) satellites (Newell et al., 2009). We applied a combined model which accounts for two main

To protect the rights of the author(s) and publisher we inform you that this PDF is an uncorrected proof for internal business use only by the author(s), editor(s), reviewer(s), Elsevier and typesetter SPi. It is not allowed to publish this proof online or in print. This proof copy is the copyright property of the publisher and is confidential until formal publication.

These proofs may contain colour figures. Those figures may print black and white in the final printed book if a colour print product has not been planned. The colour figures will appear in colour in all electronic versions of this book.

B978-0-12-821366-7.00005-6, 00005

t0010 **Table 6.1** Geographic and geomagnetic locations of the Greenland stations and conjugate points of Antarctic stations based on the IGRF for epoch 2015 (https://omniweb.gsfc.nasa.gov/vitmo/cgm.html).

Greenland Antarctica	Code	Geographic Lat.	Location lang.	Geomagnetic lat.	Conjugate lang.
	PG0	−83.67	88.68	78.7	38.2
	PG1	−84.50	77.20	77.3	37.3
	PG2	−84.42	57.95	75.5	39.1
	PG3	−84.81	37.63	73.8	36.6
	PG4	−83.34	12.25	71.1	36.1
	PG5	−81.96	05.71	69.7	37.0
Thule	THL	77.47	290.77	84.4	27.5
Savissivik	SVS	76.02	294.90	82.7	31.2
Kullorsuaq	KUV	74.57	302.82	80.4	40.3
Upernavik	UPN	72.78	303.85	78.6	38.7
Umanaq	UMQ	70.68	307.87	76.0	41.2
Godhavn	GDH	69.25	306.47	74.8	38.2
Attu	ATU	67.93	306.43	73.5	37.1
S. Stromfjord	STF	67.02	309.28	72.1	40.0
Sukkertoppen	SKT	65.42	307.10	70.9	36.4
Godthab	GHB	64.17	308.27	69.5	37.1
Frederikshab	FHB	62.00	310.32	66.9	38.4

contributors: solar photo-ionization and auroral electron precipitation. A contribution of electron precipitation is computed using the empirical model developed by Robinson et al. (1987) that relates particle flux and energy output to conductance.

p0980 Here, we compare the results of conjugate observations of such types of ULF disturbances as TCVs, Pc5 waves, SCs, and MPEs at high latitudes.

s0200 *6.3.5.2 Magnetospheric global FAC systems*

p0985 Numerous studies of large-scale magnetospheric FACs were performed using magnetic field gradients measured by low-orbiting satellites (Christiansen et al., 2002). The statistical results obtained correspond to a quasisteady (as compared with the Alfvénic time) case. Typically, empirical modeling of quasisteady magnetosphere-ionosphere current system indicated that these FACs are driven by a voltage generator. Here, we mention just a few. The study of Haraguchi et al. (2004) statistically examined the dependence of the intensities of dayside large-scale FACs on the ionospheric conductance using DMSP-F7 satellite data. In the dayside region, the intensity of R1 FAC (current flows into/away the ionosphere in the prenoon/postnoon sector) and cusp (R0) currents had a high correlation with ionospheric conductivity, suggesting that these FACs are driven by a voltage-like source. Shi et al. (2010) statistically investigated features of the FAC distribution in the plasma-sheet boundary layers in the magnetotail using the curlometer

To protect the rights of the author(s) and publisher we inform you that this PDF is an uncorrected proof for internal business use only by the author(s), editor(s), reviewer(s), Elsevier and typesetter SPi. It is not allowed to publish this proof online or in print. This proof copy is the copyright property of the publisher and is confidential until formal publication.

These proofs may contain colour figures. Those figures may print black and white in the final printed book if a colour print product has not been planned. The colour figures will appear in colour in all electronic versions of this book.

technique to calculate the current from four-point magnetic field measurements. The occurrence and polarities of FACs in the Northern hemisphere were found to be different from those in the Southern hemisphere. The interhemispheric difference between the FAC densities suggests that a source of these currents must be a voltage generator. These observational results match the model prediction of nonresonant driving of FACs.

s0205 *6.3.5.3 Traveling convection vortices*

p0990 Traveling convection vortices (TCVs) are specific daytime high-latitude structures driven by localized FACs (Friis-Christensen et al., 1988; Engebretson et al., 2013). The terrestrial manifestation of a TCV is an isolated magnetic impulse event (MIE)—a perturbation of the geomagnetic field with a duration of ∼5–10 min and amplitude of ∼100 nT (Vorob'ev, 1993). The typical double vortex TCV structure of Hall currents is formed around a pair of upward and downward FACs between the ionosphere and the magnetosphere (McHenry and Clauer, 1987). The physical mechanism of excitation of a TCV is not uniquely determined. Various driving mechanisms were claimed, such as the pulsed reconnection of the interplanetary and magnetospheric magnetic fields (Lanzerotti et al., 1990), pulsed variations in the dynamic pressure of the solar wind (Glasmeier, 1992), sporadic regions of hot plasma in the ion foreshock (hot flow anomalies) (Murr and Hughes, 2003), etc.

p0995 As an example, we consider the transient TCV events on January 19, 2013 at 1430 and 1730 UT triggered by a weak solar wind pressure increase (Kim et al., 2015). In Fig. 6.14, one can see a remarkable amplitude-phase similarity between magnetic variations in Antarctica and Greenland. A bipolar vortex-like structure is clearly seen in the ionospheric convection flow in both hemispheres. Fig. 6.15 shows the latitudinal profile of TCV amplitude determined as the extreme value of Max$B_x(t)$-Min$B_x(t)$ during the time interval 1420–1450 UT. The maximal intensity in the Northern hemisphere, ∼140 nT, is observed at $\Phi = 72$ degrees (STF). A maximum in the Southern hemisphere is hard to evaluate because of the very limited number of stations. Anyway, the difference is not more than 20%. At the same time, the contrast between conductances is about an order of magnitude. Thus, interhemispheric properties of this TCV event rather correspond to the current generator regime.

p1000 Earlier observational studies (Kim et al., 2013) of interhemispheric conjugate behavior of MIE/TCVs at high latitudes attempted to reveal how a difference in ionospheric conductivity can play a role in creating asymmetry in TCV structures. The statistical study of Lanzerotti et al. (1991), which used data from the Iqaluit-South Pole conjugate pair, found that TCVs/MIEs were of similar magnitude in the two hemispheres. A study of TCVs at the same conjugate pair by Murr et al. (2002) showed that the amplitudes of the magnetic perturbations were similar in the two hemispheres in the sunlit and dark ionospheres. Lam and Rodger (2004) also observed that conjugate TCVs were of similar intensity in both hemispheres regardless of any difference in conductivity. They found no

To protect the rights of the author(s) and publisher we inform you that this PDF is an uncorrected proof for internal business use only by the author(s), editor(s), reviewer(s), Elsevier and typesetter SPi. It is not allowed to publish this proof online or in print. This proof copy is the copyright property of the publisher and is confidential until formal publication.

These proofs may contain colour figures. Those figures may print black and white in the final printed book if a colour print product has not been planned. The colour figures will appear in colour in all electronic versions of this book.

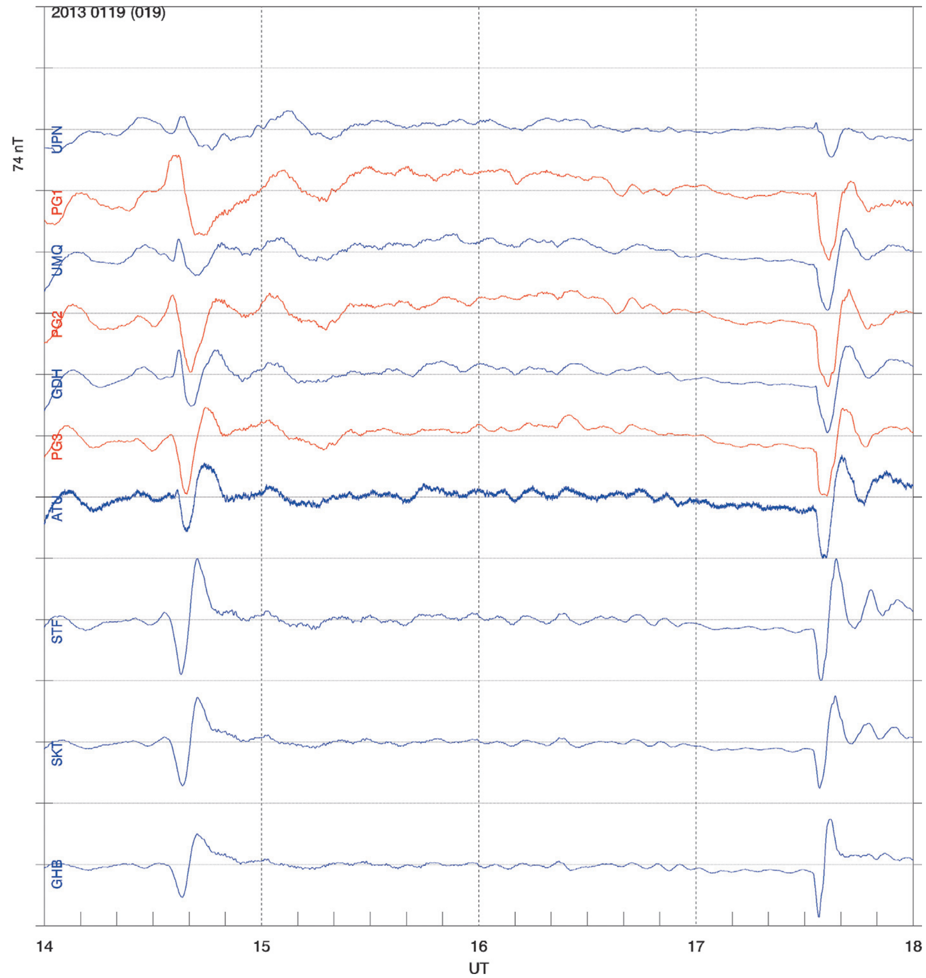

f0075 **Fig. 6.14** Stacked magnetograms (B_x component) from conjugate pairs of stations in Antarctica (*red lines*) and Greenland (*blue lines*) on January 19, 2013.

statistical difference between events occurring during conditions when one hemisphere was dark and other events when both were dark or light. Based on these observational results, it seems likely that TCVs are to be associated with a current generator.

p1005 Thus, according to the model, TCVs are to be excited at a resonant field line. However, TCV waveforms appear rather as impulsive or heavily damped oscillations. Nonetheless, it is possible that resonant effects play a significant role in the TCV formation. Though TCVs are generated by some extra-magnetospheric transients, the "epicenters" of TCV-associated FACs are found well inside the magnetosphere (Moretto and Yahnin, 1998), but not at the magnetopause. Numerical 3D modeling also showed

To protect the rights of the author(s) and publisher we inform you that this PDF is an uncorrected proof for internal business use only by the author(s), editor(s), reviewer(s), Elsevier and typesetter SPi. It is not allowed to publish this proof online or in print. This proof copy is the copyright property of the publisher and is confidential until formal publication.

These proofs may contain colour figures. Those figures may print black and white in the final printed book if a colour print product has not been planned. The colour figures will appear in colour in all electronic versions of this book.

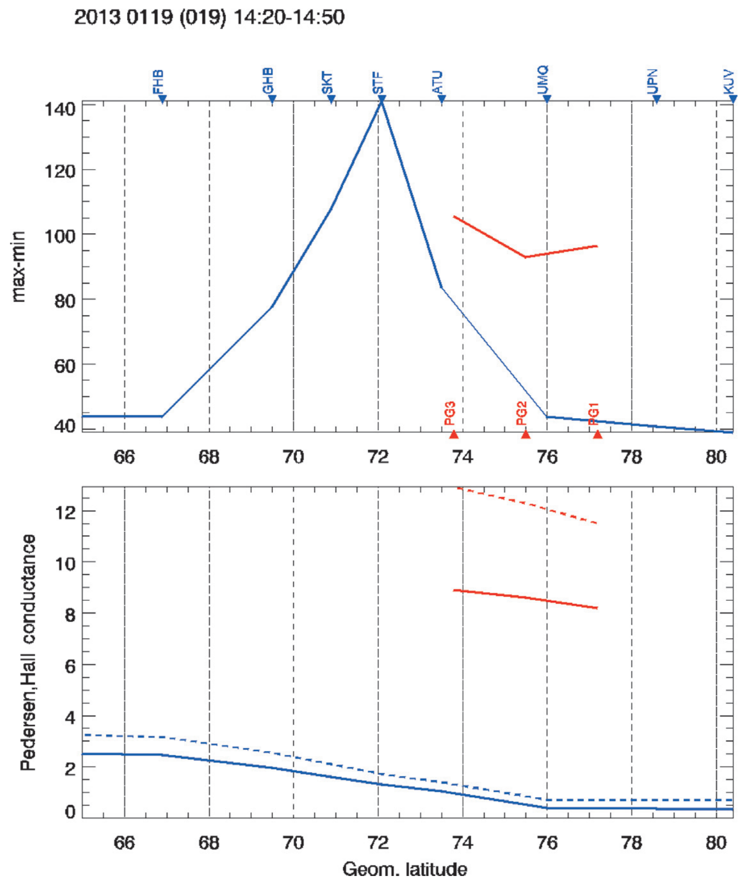

f0080 **Fig. 6.15** (*Top panel*) The latitudinal profile of TCV amplitude determined as the extreme value of Max$B_x(t)$-Min$B_x(t)$ during the time interval 1420–1450 UT, January 19, 2013 in Antarctica (*red lines*) and Greenland (*blue lines*). (*Bottom panel*) The latitudinal profile of Pedersen (*solid lines*) and Hall (*dotted lines*) conductances in Antarctica (*red lines*) and Greenland (*blue lines*).

that the generation of TCVs and the associated FACs by an interplanetary tangential discontinuity originated well inside the magnetopause (Chen et al., 2000). A possible way to reconcile the intermagnetospheric TCV response with a magnetosheath source is the assumption that the FACs which drive the TCV are produced in the Alfvén resonance region, where the initial impulse duration matches the field line eigenperiod, that is, $\tau \simeq T_A$. The actual driving time of a TCV is less than the time to reach the resonance saturation, $T_A Q$, but a TCV still can be excited because the driver intensity is much stronger than that of monochromatic Pc5 wave drivers. Thus, TCVs are likely a spatially localized phenomenon, and most probably associated with a nearly standing resonant Alfvénic mode. Therefore, the match of its conjugate features to the current generator agrees with the theoretical predictions for resonant driving of the magnetospheric Alfvén resonator.

To protect the rights of the author(s) and publisher we inform you that this PDF is an uncorrected proof for internal business use only by the author(s), editor(s), reviewer(s), Elsevier and typesetter SPi. It is not allowed to publish this proof online or in print. This proof copy is the copyright property of the publisher and is confidential until formal publication.

These proofs may contain colour figures. Those figures may print black and white in the final printed book if a colour print product has not been planned. The colour figures will appear in colour in all electronic versions of this book.

s0210 #### 6.3.5.4 Pc5 waves

p1010 The consideration of the current/voltage dichotomy for ULF waves (Pc3–5 pulsations) should be done with great care. In general, the field of ULF waves is composed of a fast magnetosonic (compressional) mode and an Alfvén mode. The transmission mechanisms of the compressional mode and Alfvén mode through the ionosphere are very different (Pilipenko et al., 2011). A FAC carried by an Alfvén wave cannot penetrate into the insulating atmosphere and instead spreads over the ionosphere, whereas the ground magnetic response is produced by the Hall currents. The magnetic field compression transported by a fast mode wave "feels" the ionosphere only weakly, and directly penetrates to the Earth's surface. Both modes, azimuthally large scale, produce a main ground response in the same B_x component. The contribution of the Alfvénic part becomes dominant in the vicinity of the peak of the resonant structure.

p1015 The north–south asymmetry of the amplitude of Pc5 pulsations was studied by Obana et al. (2005) using magnetic field data from one pair of the conjugate Kotzebue-Macquarie Island stations at $L \simeq 5.4$. The power ratio showed an "offset," probably caused by a regular bias of the statistical position of the wave resonant peak and the station location. The relative stability of the offset during seasonal variations may provide indirect evidence of the independence of the ground magnetic signal on the ionospheric conductance. A specific difficulty in analysis of conjugate studies of Pc5 pulsations is that resonant frequency-dependent amplification occurs in a small latitudinal region (about a few hundred kilometers). Conjugate observation results are strongly influenced by uncertainties in the difference between the pulsation resonant peak and an observation site. Therefore, any conclusion on Pc5 asymmetry demands a thorough preliminary determination of resonant wave structure in both hemispheres.

p1020 An example of this approach from Pilipenko et al. (2021) is given below. Spectral analysis of magnetometer data is made in a running 30-min window. The spectra of horizontal components for all stations in both hemispheres were calculated, and the central frequency band of recorded Pc5 waves has been identified. Latitudinal plots of $B_x(\Phi)$ spectral power at the central frequency of the selected band depending on geomagnetic latitude Φ were constructed. These plots enable us to compare the amplitudes of spatial peaks at two conjugate stations, where the maximum was observed. At the same time, from the OP model the ionospheric conductances were estimated. Using these values, we compare the observed ratio with the theoretical predictions. Here, we present contrasting Pc5 events during the Northern summer and Northern winter.

p1025 Stacked magnetograms of the B_x component from conjugate pairs of stations during the Northern winter event on January 25, 2016 are shown in Fig. 6.16. Quasimonochromatic Pc5 waves appeared during 06–20 UT in the recovery phase of a weak substorm with onset at ~07 UT. Signatures of field line resonance can be seen even from visual inspection: the localized amplitude of magnetic variations at GDH-PG3 stations, apparent poleward propagation, and dominance of the B_x component over the B_y component (not shown).

To protect the rights of the author(s) and publisher we inform you that this PDF is an uncorrected proof for internal business use only by the author(s), editor(s), reviewer(s), Elsevier and typesetter SPi. It is not allowed to publish this proof online or in print. This proof copy is the copyright property of the publisher and is confidential until formal publication.

These proofs may contain colour figures. Those figures may print black and white in the final printed book if a colour print product has not been planned. The colour figures will appear in colour in all electronic versions of this book.

B978-0-12-821366-7.00005-6, 00005

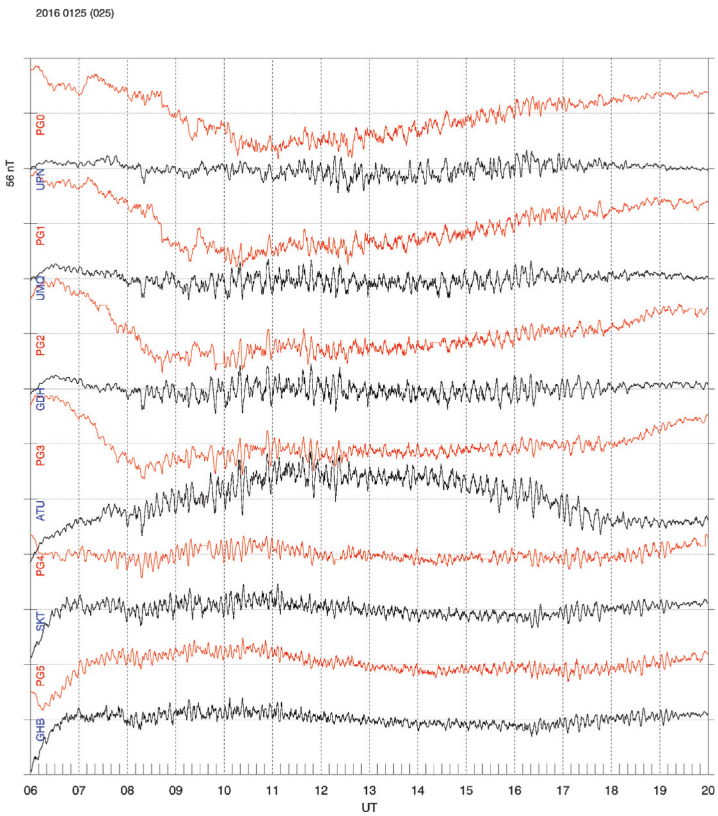

f0085 **Fig. 6.16** Stacked magnetograms of the B_x component from conjugate pairs of stations in Antarctica (*red lines*) and Greenland (*blue lines*) during the Northern winter event on January 25, 2016.

p1030 Spectra of the B_x component (not shown) demonstrate the occurrence of a spectral peak in the band between 2.0 and 2.5 mHz at most stations in both hemispheres, so the latitudinal structure of the spectral power of monochromatic Pc5 waves is examined at this frequency. The latitudinal distribution of spectral power along the profile has a maximum at $\Phi \simeq 75$ degrees in both hemispheres (Fig. 6.17). Spectral power in the Northern hemisphere is larger than that in the Southern hemisphere, but just weakly, ~20%–40%. The predicted ionospheric height-integrated conductances are around $\Sigma^{(S)} \simeq 5-6$ S, and $\Sigma^{(N)} \simeq 1$ S.

p1035 Stacked magnetograms of the B_x component from conjugate pairs of stations for the Northern summer event on June 13, 2016 are shown in Fig. 6.18. Quasimonochromatic Pc5 waves appeared between 09 and 15 UT. Even from a visual inspection of magnetograms, one can see a regular increase of the dominant frequency from 2.5 mHz at high latitudes (PG2-UMQ) toward 3.5 mHz at lower latitudes (PG5-SKT). During the 13–14 UT interval, the latitudinal peaks of spectral power at $f = 2.0-2.5$ mHz are at the same

To protect the rights of the author(s) and publisher we inform you that this PDF is an uncorrected proof for internal business use only by the author(s), editor(s), reviewer(s), Elsevier and typesetter SPi. It is not allowed to publish this proof online or in print. This proof copy is the copyright property of the publisher and is confidential until formal publication.

These proofs may contain colour figures. Those figures may print black and white in the final printed book if a colour print product has not been planned. The colour figures will appear in colour in all electronic versions of this book.

B978-0-12-821366-7.00005-6, 00005

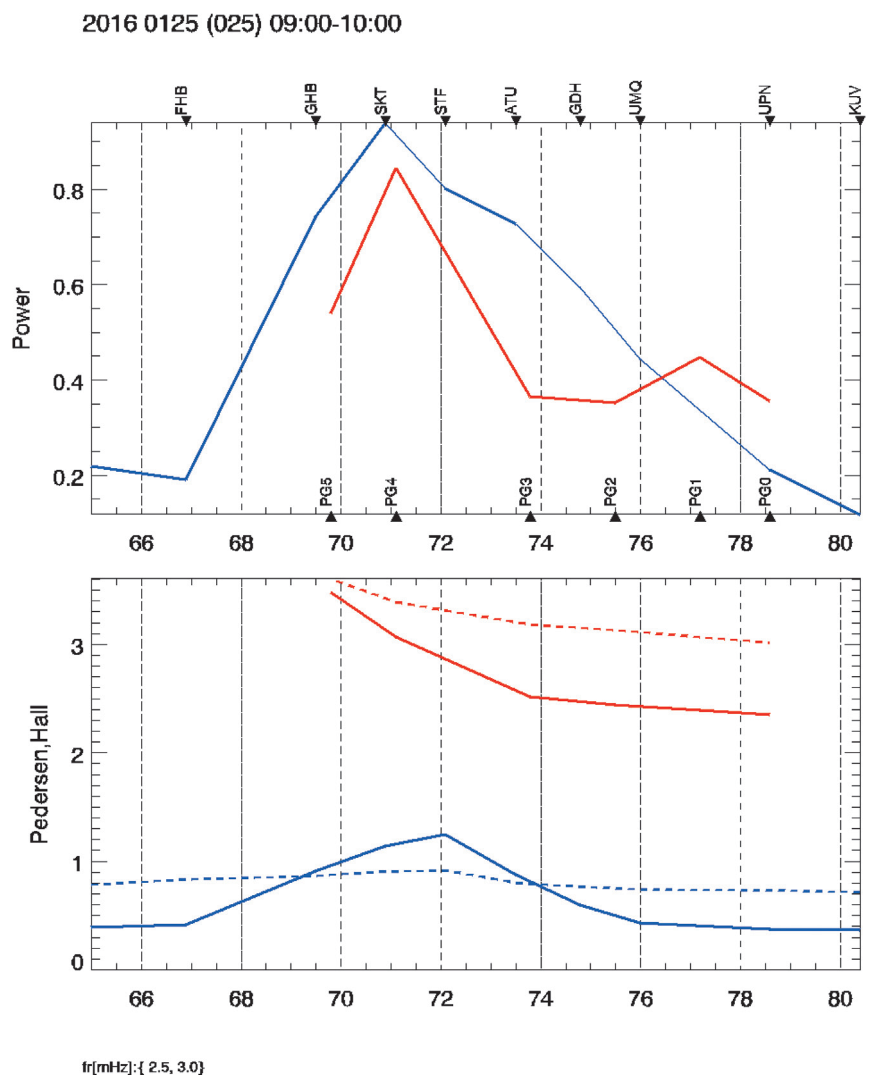

f0090 **Fig. 6.17** (*Top panel*) The latitudinal distribution of spectral power (*X* component) in the 2.0–2.5 mHz band along the profile in the Northern (*blue lines*) and Southern (*red lines*) hemispheres during the Northern winter event on January 25, 2016. (*Bottom panel*) The predicted ionospheric height-integrated Pedersen (*solid lines*) and Hall (*dashed lines*) conductances in Antarctica (*red lines*) and Greenland (*blue lines*).

geomagnetic latitude in both hemispheres, around 74 degrees (ATU/PG3) (Fig. 6.19). The interhemispheric contrast between ionospheric conductances is rather substantial, $\Sigma_H^{(N)} \simeq 11$ S, whereas $\Sigma_H^{(S)} \simeq 0.8$ S. The profile of the ionospheric conductance is weakly dependent on latitude, and strong gradients are absent. Despite the strong asymmetry of the ionospheric conductance, the magnetic field spectral power is nearly the same in both

To protect the rights of the author(s) and publisher we inform you that this PDF is an uncorrected proof for internal business use only by the author(s), editor(s), reviewer(s), Elsevier and typesetter SPi. It is not allowed to publish this proof online or in print. This proof copy is the copyright property of the publisher and is confidential until formal publication.

These proofs may contain colour figures. Those figures may print black and white in the final printed book if a colour print product has not been planned. The colour figures will appear in colour in all electronic versions of this book.

B978-0-12-821366-7.00005-6, 00005

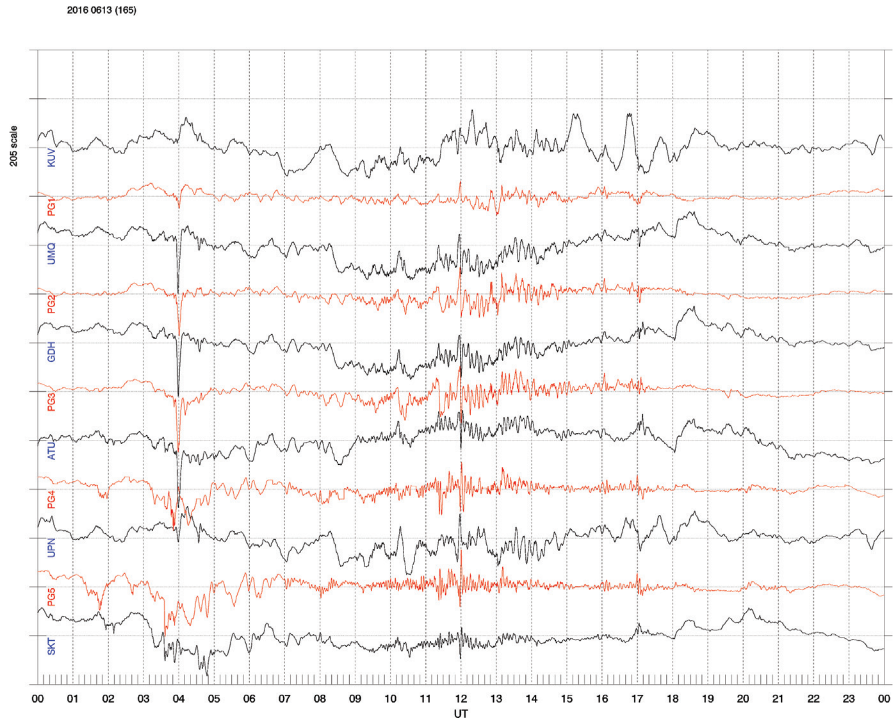

f0095 **Fig. 6.18** Stacked magnetograms of the B_x component from conjugate pairs of stations in Antarctica (*red lines*) and Greenland (*blue lines*) for the Northern summer event on June 13, 2016.

hemispheres, $B^{(N)} \simeq B^{(S)}$. Thus, the interhemispheric contrast between the Pc5 amplitudes is much less than the contrast between ionospheric conductivities. The Pc5 wave excitation is much closer to the current generator regime than to the voltage generator regime.

s0215 *6.3.5.5 High-latitude SC impulses*

p1040 A sudden commencement (SC) is a complicated large-scale transient response of the magnetosphere-ionosphere system to an interplanetary shock. It consists of a magnetic field compression transported to the ground by a fast compressional mode wave and a global vortex-like disturbance produced by an FAC system at the magnetopause. The SC-associated compression of the magnetosphere can excite damped Psc5 pulsations in the magnetosphere localized at a latitudinally narrow resonant magnetic shell where the impulse duration $\tau \simeq T_A$. Beyond this narrow region, no periodic resonant response to the SC pulse is observed. Thus, the SC main impulse is a transient FAC stimulated by an interplanetary shock and predominantly it corresponds either to the condition $\tau \gg T_A$ (at low latitudes, where $T_A < 1$ min) or $\tau \ll T_A$ (at high latitudes, where $T_A \simeq$ 5−10 min). Formally, low latitude SC observations are to be treated as an example of

ToshiNishimura, 978-0-12-821366-7

To protect the rights of the author(s) and publisher we inform you that this PDF is an uncorrected proof for internal business use only by the author(s), editor(s), reviewer(s), Elsevier and typesetter SPi. It is not allowed to publish this proof online or in print. This proof copy is the copyright property of the publisher and is confidential until formal publication.

These proofs may contain colour figures. Those figures may print black and white in the final printed book if a colour print product has not been planned. The colour figures will appear in colour in all electronic versions of this book.

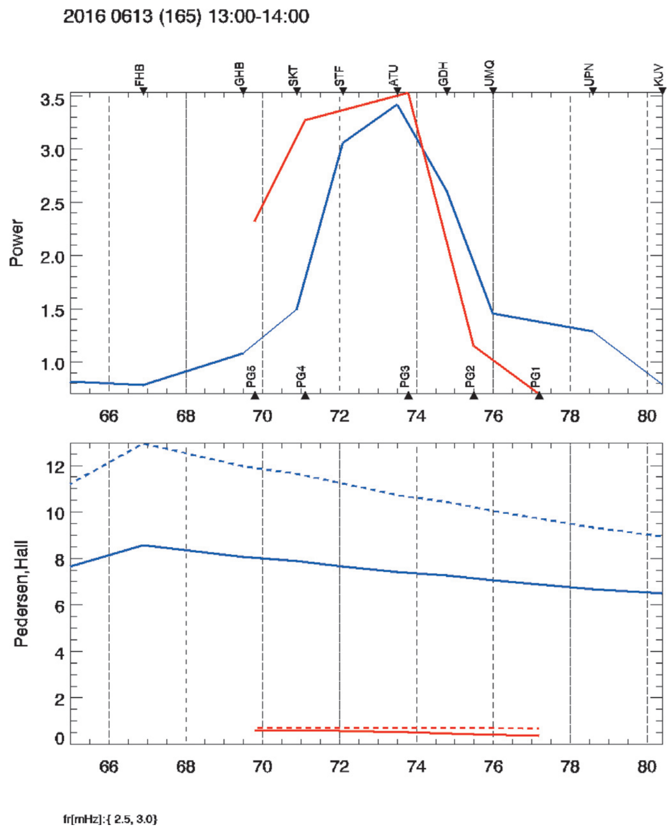

f0100 **Fig. 6.19** (*Top panel*) The latitudinal distribution of spectral power (*X* component) in the 2.0–2.5 mHz band along the profile in the Northern (*blue lines*) and Southern (*red lines*) hemispheres during the Northern summer event on June 13, 2016. (*Bottom panel*) The predicted ionospheric height-integrated Pedersen (*solid lines*) and Hall (*dashed lines*) conductances in Antarctica (*red lines*) and Greenland (*blue lines*).

a quasi-DC excitation. Studies at low latitudes ($L < 3$) indeed revealed an interhemispheric difference in SC signatures: their amplitude was significantly larger in the summer hemisphere than in the winter one (Yumoto et al., 1996). Shinbori et al. (2012) also found that the size of the diurnal variation of the SC main impulse increased significantly during the summer, compared with that during the winter. Based on the seasonal and interhemispheric variations of SCs at low latitudes, it may be concluded that the SC in this region is caused by a voltage generator rather than a current generator. The regime of a voltage generator is natural for a nonresonant quasi-DC disturbance (Pilipenko et al., 2019).

p1045 However, in contrast to low latitudes, for an SC pulse at high latitudes ($L > 6$), the inverse condition takes place, $\tau \ll T_A$. Here, we present typical SC events on a quiet

To protect the rights of the author(s) and publisher we inform you that this PDF is an uncorrected proof for internal business use only by the author(s), editor(s), reviewer(s), Elsevier and typesetter SPi. It is not allowed to publish this proof online or in print. This proof copy is the copyright property of the publisher and is confidential until formal publication.

These proofs may contain colour figures. Those figures may print black and white in the final printed book if a colour print product has not been planned. The colour figures will appear in colour in all electronic versions of this book.

background during summer and winter, and determine from conjugate station data the ratio between amplitudes of pulses $B_x^{(N)}/B_x^{(S)}$ at conjugate pairs of stations in Antarctica and Greenland. The magnetospheric Alfvén conductance is supposed not to differ considerably throughout the magnetosphere, $\Sigma_A^{(N)} \simeq \Sigma_A^{(S)} \simeq 1$ S.

p1050 We first present the Northern winter event that occurred on January 7, 2014, 15 UT (Fig. 6.20, top panel). According to the IRI-2016 model, for the central PG3 station in the Southern hemisphere $\Sigma_P^{(S)} \simeq 5.0$ S and $\Sigma_H^{(S)} \simeq 6.0$ S. For the conjugate station ATU in the Northern hemisphere $\Sigma_P^{(N)} \simeq 2.4$ S, and $\Sigma_H^{(N)} \simeq 2.1$ S. In this event, the contrast between the Northern and Southern conductances is not so strong. There is an additional factor that may obscure the observed relationship between the ground magnetic response and the ionospheric conductance, which should be taken into account. Though the model considered in Section 6.2 is homogeneous, in reality Q7 the plasma density N_e in the upper ionosphere at the sunlit end of a field line probably should be higher than at the dark end. As a result, the Alfvén wave conductance, $\Sigma_A \propto \sqrt{N_e}$, must be higher at the sunlit end. Thus, the contrast in the ratio Σ_P/Σ_A, which determines the reflection condition and ground response, is to be less distinct between (N) and (S) ionospheres. Here, as a proxy of plasma density in the upper ionosphere, N_e, total electron content (TEC) maps from GPS receivers have been used (http://vt.superdarn.org). Based on very sparse observations in Greenland and Antarctica, TEC in the Northern hemisphere is ~12 TECu, while in the Southern hemisphere TEC is ~15 TECu. Then, Eq. (6.75) gives us $B_x^{(N)}/B_x^{(S)} \simeq 0.5$. The correction for the asymmetry of $\Sigma_A^{(N)}/\Sigma_A^{(S)} \simeq \sqrt{TEC^{(N)}/TEC^{(S)}} \simeq 0.9$ does not modify this estimate noticeably. Thus, the model predicts that by the order of magnitude the amplitudes of pulses in conjugate ionospheres are to be about the same. The observed amplitudes of the SC pulse at station pairs GDH-PG2, ATU-PG3, and SKT-PG4 are indeed about the same within 15%.

p1055 Then, we consider the typical Northern summer event on June 7, 2014, 17 UT (Fig. 6.20, bottom panel). For the central PG3 station in the Southern hemisphere, the ionospheric conductances estimated with the use of the IRI-2016 model are as follows: $\Sigma_P^{(S)} \simeq 0.2$ S and $\Sigma_H^{(S)} \simeq 0.2$ S. For the conjugate station ATU in the Northern hemisphere, the ionospheric conductances are: $\Sigma_P^{(N)} \simeq 6.8$ S, and $\Sigma_H^{(N)} \simeq 8.8$ S. Therefore, it is reasonable to assume that $\overline{\Sigma}_P^{(N)} \gg 1$ and $\overline{\Sigma}_P^{(S)} \ll 1$. According to the TEC maps for this event, the TEC in the Northern hemisphere is ~15 TECu, while in the Southern hemisphere it is below 5 TECu. Then, Eq. (6.75) gives us $B_x^{(N)}/B_x^{(S)} \simeq 6.5$. The asymmetry of $\Sigma_A^{(N)}/\Sigma_A^{(S)} \simeq \sqrt{TEC^{(N)}/TEC^{(S)}} \simeq 1.7$ decreases this estimate down to ~3.8. This prediction matches surprisingly well the observed ratio between magnetic responses in conjugate ionospheres: for the ATU-PG3 pair the ratio is ~3.8.

To protect the rights of the author(s) and publisher we inform you that this PDF is an uncorrected proof for internal business use only by the author(s), editor(s), reviewer(s), Elsevier and typesetter SPi. It is not allowed to publish this proof online or in print. This proof copy is the copyright property of the publisher and is confidential until formal publication.

These proofs may contain colour figures. Those figures may print black and white in the final printed book if a colour print product has not been planned. The colour figures will appear in colour in all electronic versions of this book.

B978-0-12-821366-7.00005-6, 00005

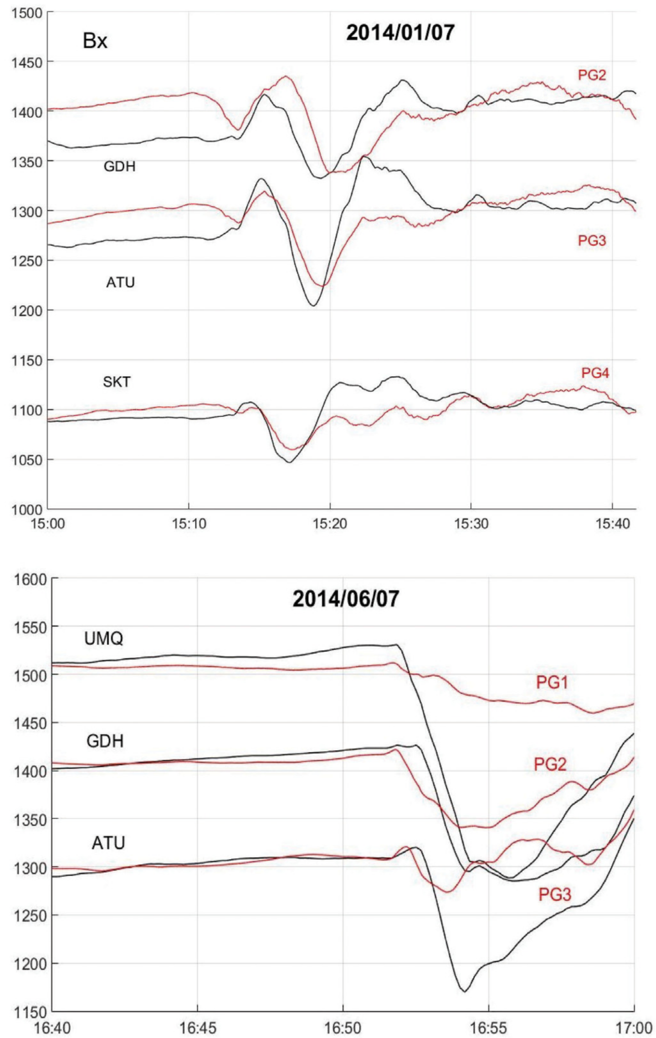

f0105 **Fig. 6.20** (*Top panel*) Stacked magnetograms from Antarctic and Greenland conjugate pairs of stations during the Northern summer SC event on June 7, 2014. (*Bottom panel*) Stacked magnetograms from Antarctic and Greenland conjugate pairs of stations during the Northern winter SC event on January 7, 2014.

s0220 *6.3.5.6 Magnetic perturbation events*

p1060 When the auroral oval expands to subauroral latitudes, impulsive MPEs with duration ~5–15 min occur during even nonstorm times and at up to 78 degrees magnetic latitude (Engebretson et al., 2019a). The MPEs appear roughly simultaneously at near

ToshiNishimura, 978-0-12-821366-7

To protect the rights of the author(s) and publisher we inform you that this PDF is an uncorrected proof for internal business use only by the author(s), editor(s), reviewer(s), Elsevier and typesetter SPi. It is not allowed to publish this proof online or in print. This proof copy is the copyright property of the publisher and is confidential until formal publication.

These proofs may contain colour figures. Those figures may print black and white in the final printed book if a colour print product has not been planned. The colour figures will appear in colour in all electronic versions of this book.

B978-0-12-821366-7.00005-6, 00005

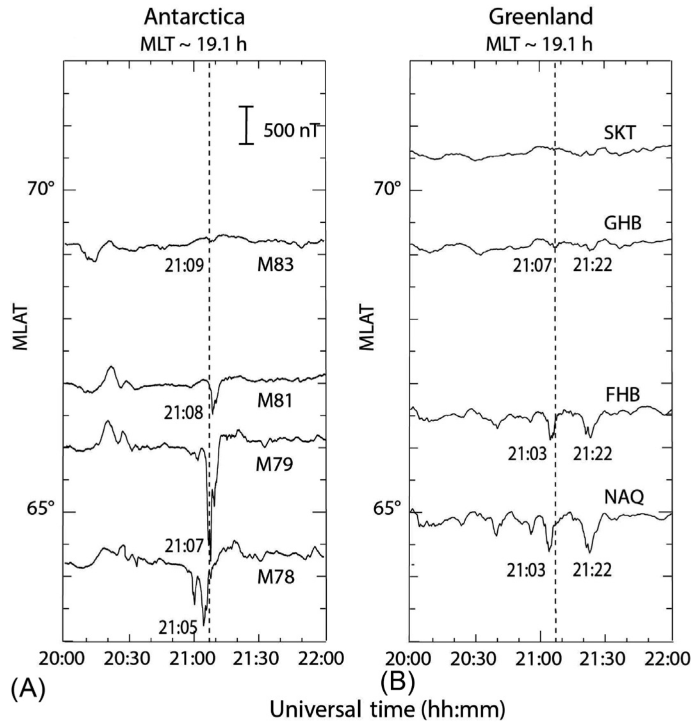

f0110 **Fig. 6.21** Magnetograms from stations in the Northern hemisphere (A) and at magnetically conjugate locations in Antarctica (B) during May 8, 2016.

magnetically conjugate locations in each hemisphere (Engebretson et al., 2019b). Here, we present data from a 2D set of ground-based magnetometers in the Northern hemisphere and magnetometers at magnetically conjugate locations in Antarctica during May 8, 2016 (Fig. 6.21). This MPE interval (2102–2130 UT) includes an extremely large $dB/dt \simeq 37.7$ nT/s at M79, but MPEs appear only from 64 to 69 degrees. Multiple substorm onsets occurred ~1–3 h before the beginning of the MPE interval. Magnetograms from BAS LPM M79 and FHB on this day show that a single B_x minimum at M79 appeared at 21:07 UT, and two B_x minima appeared at FHB at 21:04 and 21:22 UT, respectively. The largest $|dB_x/dt|$ excursion at FHB was substantial (6.7 nT/s), but was a factor of ~5 smaller than that at M79.

p1065 The amplitude and location data for the MPE during this interval can be used to estimate its latitudinal and longitudinal scale size. Both B_x and the derivatives in each component at the Antarctic stations were highly localized in MLAT: the maximum $|dB_x/dt|$ value decreased to less than half its maximal value within 1–1.7 degrees. The latitudinal distances ranged from 100 to 200 km, and for the two somewhat less closely spaced West Greenland stations at nearly the same magnetic longitude, the latitudinal distance was

To protect the rights of the author(s) and publisher we inform you that this PDF is an uncorrected proof for internal business use only by the author(s), editor(s), reviewer(s), Elsevier and typesetter SPi. It is not allowed to publish this proof online or in print. This proof copy is the copyright property of the publisher and is confidential until formal publication.

These proofs may contain colour figures. Those figures may print black and white in the final printed book if a colour print product has not been planned. The colour figures will appear in colour in all electronic versions of this book.

~200 km. These latitudinal distances are roughly comparable with the ~275 km 2D half-amplitude radius calculated for several events in Arctic Canada using the SECs technique by Engebretson et al. (2019a).

p1070 The first MPE observed in Greenland occurred within ~3 min of the much larger MPE observed in Antarctica, and conversely there was no evidence of the second Greenland MPE at any of the Antarctic stations. Thus, for both MPEs there was an apparent lack of conjugacy. However, at least some of this lack of conjugacy might be attributed to longitudinal localization of both MPEs: BAS LPM stations M79 and M81 were located ~9 degrees in magnetic longitude west of the conjugate point of FHB, at distances of ~ 430 km.

p1075 During the interval under study, both perturbation and derivative amplitudes were consistently larger by a factor of ~3 in the Southern hemisphere than in the Northern hemisphere at comparable latitudes (Fig. 6.22A and B). Fig. 6.22C shows the ionospheric conductances calculated using an updated AMIE procedure based on an empirical model parameterized by solar zenith angle and the solar radio flux index, F10.7 (Cousins et al., 2015). This augmented model contributed only negligible additional conductances because the modeled auroral zone was located below the latitude range of the available stations.

p1080 It has been suggested that MPEs are driven by localized FACs, which transfer an image of a "spacequake" in the magnetotail to the high-latitude nightside ionosphere. However, the exact mechanism of FAC generation and specific channel of the disturbance propagation have not been established. Current/voltage generator properties may be helpful to reveal this mechanism. Inverse interhemispheric patterns are evident during northern summer events (not shown here): magnetic perturbations and derivatives were mostly larger in the Southern hemisphere, and conductances were much larger in the Northern hemisphere. Northern hemisphere conductances based on the AMIE model increased relatively smoothly with MLT, while Southern hemisphere conductances were nearly constant. These relations indicate that for MPEs the voltage generator model is not applicable. On the other hand, the difference between Northern and Southern amplitudes is too large to fit the current generator regime, even under the known uncertainties in the modeled conductances.

s0225 6.3.6 Discussion: Additional factors influencing ground magnetometer observations

p1085 The simple consideration in this review necessarily neglected some, hopefully of secondary importance, factors. The factors that may complicate the examination of ionospheric conductance effect in magnetically conjugate points are (a) the differing effects on ground conductivity of coastlines and oceans in the north versus ice sheets in the south and (b) the fact that Antarctic stations are situated at 13–18 degrees higher geographic latitude than Arctic stations at similar MLAT.

To protect the rights of the author(s) and publisher we inform you that this PDF is an uncorrected proof for internal business use only by the author(s), editor(s), reviewer(s), Elsevier and typesetter SPi. It is not allowed to publish this proof online or in print. This proof copy is the copyright property of the publisher and is confidential until formal publication.

These proofs may contain colour figures. Those figures may print black and white in the final printed book if a colour print product has not been planned. The colour figures will appear in colour in all electronic versions of this book.

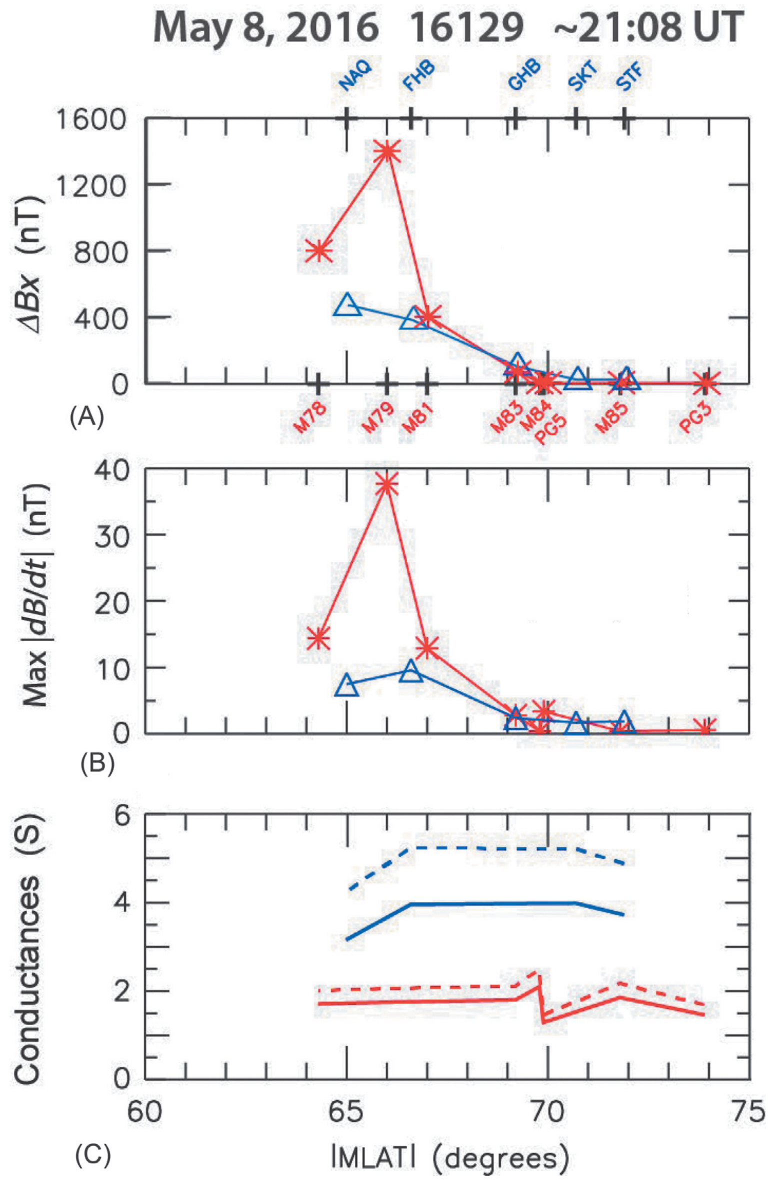

f0115 **Fig. 6.22** Latitudinal profile of MPE amplitudes (A) and derivative amplitudes (B) in the Southern and Northern hemispheres during the MPE of May 8, 2016. (C) Ionospheric conductances calculated using an updated AMIE procedure. *Solid lines* and *dashed lines* denote Pedersen and Hall conductances, respectively.

To protect the rights of the author(s) and publisher we inform you that this PDF is an uncorrected proof for internal business use only by the author(s), editor(s), reviewer(s), Elsevier and typesetter SPi. It is not allowed to publish this proof online or in print. This proof copy is the copyright property of the publisher and is confidential until formal publication.

These proofs may contain colour figures. Those figures may print black and white in the final printed book if a colour print product has not been planned. The colour figures will appear in colour in all electronic versions of this book.

B978-0-12-821366-7.00005-6, 00005

p1090 The conclusion that Pc5 wave interhemispheric properties correspond to the current generator regime does not mean that Pc5 excitation efficiency in the magnetosphere does not depend on the ionospheric conductivity. By contrast, it seems reasonable that a low damping of Alfvén field line oscillations in the regions with elevated ionospheric conductance is favorable for the Pc5 wave excitation (Sutcliffe and Rostoker, 1979).

p1095 At high latitudes, the presence of the auroral acceleration region (AAR) must be taken into account upon consideration of the magnetospheric driver's internal resistance and the load resistance. A potential drop along auroral field lines can be modeled with the Ohm-type nonlocal current-voltage relationship (Fedorov et al., 2001). A special consideration is needed to reveal the influence of the mirror resistance along auroral field lines on interhemispheric properties of disturbances at these latitudes.

p1100 The model considered here has a passive ionosphere, whose conductances do not evolve due to the current/voltage imposed on the ionosphere. However, a very intense FAC can modify the ionosphere via plasma transport by Alfvén wave (Belakhovsky et al., 2016) or modulated precipitation of particles (Spanswick et al., 2005). An SC impulse can trigger sporadic precipitation of energetic electrons (Rosenberg et al., 1980), which may locally modify the ionospheric conductance. However, during daytime, such precipitation is not strong enough to modify considerably the ionospheric global parameters. Such extreme events of the ionospheric conductance modification by a magnetospheric driver are not considered in the linear theory. A steep gradient of the ionospheric conductance, for example, at the auroral oval boundary or cusp boundary, also neglected in the above consideration, can substantially distort the ground magnetic response (Glasmeier et al., 1984).

p1105 The above consideration is an element of the more global problem of the significance of the ionosphere for the a coupled magnetosphere-ionosphere system. Though it is generally thought that the occurrence of substorms is externally controlled by some instability in the magnetotail, Liou et al. (2018) provided a strong argument that the ionosphere plays an active role in the occurrence of substorms. Statistical analysis of UV images indicated that substorm onsets occurred more frequently when the ionosphere was dark, and in regions where the Earth's magnetic field is largest. There is mounting evidence suggesting a relationship between solar illumination and the occurrence frequency of auroral acceleration events, which produce discrete arcs (Newell et al., 1996). These facts suggest that auroral substorms occur more frequently when the ionospheric conductivity is lower.

s0230 6.3.7 Conclusion

p1110 Here, we have highlighted an important aspect of the magnetosphere-ionosphere interaction, which should be taken into account when considering the ground response to magnetospheric FAC driving. A simple box model of the magnetosphere predicts that

To protect the rights of the author(s) and publisher we inform you that this PDF is an uncorrected proof for internal business use only by the author(s), editor(s), reviewer(s), Elsevier and typesetter SPi. It is not allowed to publish this proof online or in print. This proof copy is the copyright property of the publisher and is confidential until formal publication.

These proofs may contain colour figures. Those figures may print black and white in the final printed book if a colour print product has not been planned. The colour figures will appear in colour in all electronic versions of this book.

B978-0-12-821366-7.00005-6, 00005

nonsteady FACs interact with the ionosphere in a different way in cases of a forced driving or resonant excitation. A quasi-DC driving of FAC corresponds to a voltage generator regime, when the ground magnetic response is proportional to the ionospheric Hall conductance. A resonant excitation corresponds to the current generator regime, when the ground magnetic response practically does not depend on the ionospheric conductance. According to the suggested conception, quasi-DC nonresonant disturbances such as global magnetospheric FAC systems and SCs at low latitudes correspond to a voltage generator. Such magnetospheric phenomena as TCVs and Pc5 waves should be considered as a resonant response of magnetospheric field lines and correspond to a current generator. For a short SC pulse at high latitudes when a conjugate ionosphere does not influence the pulse interaction with the ionosphere of interest, the interhemispheric asymmetry of pulse amplitude in the general does not correspond either to the current or voltage generator. The typical ULF events shown here support the outline of the classification scheme that enabled us to resolve the current/voltage dichotomy. The aspects of the current/voltage dichotomy presented here should be taken into account when considering the magnetosphere-ionosphere interaction, and can be applied to improve global MHD simulations.

Acknowledgments

This study is supported by a grant 20-05-00787 from the Russian Fund for Basic Research (ENF), and the US National Science Foundation grants PLR-1744828 to Virginia Tech (MDH and SC) and AGS-2013648 to the Augsburg University (VAP and MJE).

References

Agostinelli, S., et al., 2003. GEANT4-a simulation toolkit. Nucl. Instrum. Methods A 506 (25), 250–303.

Allison, J., Amako, K., Apostolakis, J., Arce, P., Asai, M., Aso, T., Bagli, E., Bagulya, A., Banerjee, S., Barrand, G.J.N.I., et al., 2016. Recent developments in Geant4. Nucl. Instrum. Methods Phys. Res. A 835, 186–225.

Alperovich, L.S., Fedorov, E.N., 2007. Hydromagnetic Waves in the Magnetosphere and the Ionosphere. vol. 353 Springer Science & Business Media. Q8

André, M., Norqvist, P., Vaivads, A., Eliasson, L., Norberg, O., Eriksson, A.I., Holback, B., 1994. Transverse ion energization and wave emissions observed by the Freja satellite. Geophys. Res. Lett. 21 (17), 1915–1918. https://doi.org/10.1029/94GL00699.

Arfken, G.B., Weber, H.J., Harris, F.E., 2012. Mathematical Methods for Physicists, seventh. Academic Press, Boston, MA, https://doi.org/10.1016/B978-0-12-384654-9.00032-3.

Artamonov, A., Mironova, I., Kovaltsov, G., Mishev, A., Plotnikov, E., Konstantinova, N., 2017. Calculation of atmospheric ionization induced by electrons with non-vertical precipitation: updated model CRAC-EPII. Adv. Space Res. 59 (9), 2295–2300.

Bahcivan, H., 2007. Plasma wave heating during extreme electric fields in the high-latitude E region. Geophys. Res. Lett. 34 (15), L15106. https://doi.org/10.1029/2006GL029236.

Bailey, D.K., 1959. Abnormal ionization in the lower ionosphere associated with cosmic-ray flux enhancements. Proc. IRE 47 (2), 255–266.

To protect the rights of the author(s) and publisher we inform you that this PDF is an uncorrected proof for internal business use only by the author(s), editor(s), reviewer(s), Elsevier and typesetter SPi. It is not allowed to publish this proof online or in print. This proof copy is the copyright property of the publisher and is confidential until formal publication.

These proofs may contain colour figures. Those figures may print black and white in the final printed book if a colour print product has not been planned. The colour figures will appear in colour in all electronic versions of this book.

Banjac, S., Herbst, K., Heber, B., 2019. The atmospheric radiation interaction simulator (ATRIS): description and validation. J. Geophys. Res. Space Phys. 124 (1), 50–67.

Banks, P.M., Nagy, A.F., 1970. Concerning the influence of elastic scattering upon photoelectron transport and escape. J. Geophys. Res. 75 (10), 1902–1910.

Banks, P.M., Chappell, C.R., Nagy, A.F., 1974. A new model for the interaction of auroral electrons with the atmosphere: spectral degradation, backscatter, optical emission, and ionization. J. Geophys. Res. 79 (10), 1459–1470.

Basu, B., Chang, T., Jasperse, J.R., 1982. Electrostatic plasma instabilities in the daytime lower ionosphere. Geophys. Res. Lett. 9 (1), 68–71. https://doi.org/10.1029/GL009i001p00068.

Basu, B., Jasperse, J.R., Robinson, R.M., Vondrak, R.R., Evans, D.S., 1987. Linear transport theory of auroral proton precipitation: a comparison with observations. J. Geophys. Res. Space Phys. 92 (A6), 5920–5932.

Basu, B., Jasperse, J.R., Strickland, D.J., Daniell Jr, R.E., 1993. Transport-theoretic model for the electron-proton-hydrogen atom aurora: 1. Theory. J. Geophys. Res. Space Phys. 98 (A12), 21517–21532.

Basu, B., Decker, D.T., Jasperse, J.R., 2001. Proton transport model: a review. J. Geophys. Res. Space Phys. 106 (A1), 93–105.

Belakhovsky, V., Pilipenko, V., Murr, D., Fedorov, E., Kozlovsky, A., 2016. Modulation of the ionosphere by Pc5 waves observed simultaneously by GPS/TEC and EISCAT. Earth Planets Space 68 (1), 1–13.

Bellan, P.M., 2008. Fundamentals of Plasma Physics. Cambridge University Press.

Berger, M.J., 1963. Monte Carlo calculation of the penetration and diffusion of fast charged particles. Methods Comput. Phys. 135. Q9

Berger, M.J., Coursey, J.S., Zucker, M.A., Chang, J., 2017. ESTAR, PSTAR, and ASTAR: Computer Programs for Calculating Stopping-Power and Range Tables for Electrons, Protons, and Helium Ions (version 2.0.1). National Institute of Standards and Technology, Gaithersburg, MD. http://physics.nist.gov/Star.

Bhatnagar, P.L., Gross, E.P., Krook, M., 1954. A model for collision processes in gases. I. Small amplitude processes in charged and neutral one-component systems. Phys. Rev. 94, 511–525. https://doi.org/10.1103/PhysRev.94.511.

Bilitza, D., Altadill, D., Truhlik, V., Shubin, V., Galkin, I., Reinisch, B., Huang, X., 2017. International reference ionosphere 2016: from ionospheric climate to real-time weather predictions. Space Weather 15 (2), 418–429.

Buneman, O., 1963. Excitation of field aligned sound waves by electron streams. Phys. Rev. Lett. 10, 285.

Cashwell, E.D., Everett, C.J., 1959. A Practical Manual on the Monte Carlo Method for Random Walk Problems. Pergamon. Q10

Chaston, C.C., Bonnell, J.W., Carlson, C.W., McFadden, J.P., Ergun, R.E., Strangeway, R.J., 2003. Properties of small-scale Alfvén waves and accelerated electrons from FAST. J. Geophys. Res. Space Phys. 108 (A4). https://doi.org/10.1029/2002JA009420.

Chen, G.X., Lin, Y., Cable, S., 2000. Generation of traveling convection vortices and field-aligned currents in the magnetosphere by response to an interplanetary tangential discontinuity. Geophys. Res. Lett. 27 (21), 3583–3586.

Chen, M.W., Lemon, C.L., Guild, T.B., Keesee, A.M., Lui, A., Goldstein, J., Rodriguez, J.V., Anderson, P. C., 2015. Effects of modeled ionospheric conductance and electron loss on self-consistent ring current simulations during the 5–7 April 2010 storm. J. Geophys. Res. Space Phys. 120 (7), 5355–5376. https://doi.org/10.1002/2015JA021285.

Choudhuri, A.R., 1998. The Physics of Fluids and Plasmas: An Introduction for Astrophysicists. Cambridge University Press. Q11

Christiansen, F., Papitashvili, V.O., Neubert, T., 2002. Seasonal variations of high-latitude field-aligned currents inferred from Ørsted and Magsat observations. J. Geophys. Res. Space Phys. 107 (A2), SMP-5.

Cousins, E.D.P., Matsuo, T., Richmond, A.D., 2015. Mapping high-latitude ionospheric electrodynamics with SuperDARN and AMPERE. J. Geophys. Res. Space Phys. 120 (7), 5854–5870.

Davidson, G.T., 1965. Expected spatial distribution of low-energy protons precipitated in the auroral zones. J. Geophys. Res. 70 (5), 1061–1068.

To protect the rights of the author(s) and publisher we inform you that this PDF is an uncorrected proof for internal business use only by the author(s), editor(s), reviewer(s), Elsevier and typesetter SPi. It is not allowed to publish this proof online or in print. This proof copy is the copyright property of the publisher and is confidential until formal publication.

These proofs may contain colour figures. Those figures may print black and white in the final printed book if a colour print product has not been planned. The colour figures will appear in colour in all electronic versions of this book.

Decker, D.T., Kozelov, B.V., Basu, B., Jasperse, J.R., Ivanov, V.E., 1996. Collisional degradation of the proton-H atom fluxes in the atmosphere: a comparison of theoretical techniques. J. Geophys. Res. Space Phys. 101 (A12), 26947–26960.

Desai, M., Giacalone, J., 2016. Large gradual solar energetic particle events. Living Rev. Solar Phys. 13 (1), 1–132.

Dimant, Y.S., Oppenheim, M.M., 2004. Ion thermal effects on E-region instabilities: linear theory. J. Atmos. Solar Terr. Phys. 66, 1639–1654. https://doi.org/10.1016/j.jastp.2004.07.006.

Dimant, Y.S., Oppenheim, M.M., 2011. Magnetosphere-ionosphere coupling through E-region turbulence: 2. Anomalous conductivities and frictional heating. J. Geophys. Res. 116 (A09), A09304. https://doi.org/10.1029/2011JA016649.

Dimant, Y.S., Sudan, R.N., 1997. Physical nature of a new cross-field current-driven instability in the lower ionosphere. J. Geophys. Res. 102, 2551–2564. https://doi.org/10.1029/96JA03274.

Drummond, W.E., 2004. Landau damping. Phys. Plasmas 11 (2), 552–560. https://doi.org/10.1063/1.1628685.

Drummond, W.E., Pines, D., 1962. Non-linear stability of plasma oscillations. Nucl. Fusion Suppl. 2. Q12

Eliasson, L., André, M., Eriksson, A., Norqvist, P., Norberg, O., Lundin, R., Holback, B., Koskinen, H., Borg, H., Boehm, M., 1994. Freja observations of heating and precipitation of positive ions. Geophys. Res. Lett. 21 (17), 1911–1914. https://doi.org/10.1029/94GL01067.

Eltrass, A., Mahmoudian, A., Scales, W.A., de Larquier, S., Ruohoniemi, J.M., Baker, J.B.H., Greenwald, R.A., Erickson, P.J., 2014. Investigation of the temperature gradient instability as the source of midlatitude quiet time decameter-scale ionospheric irregularities: 2. Linear analysis. J. Geophys. Res. Space Phys. 119 (6), 4882–4893. https://doi.org/10.1002/2013JA019644.

Emery, B.A., Coumans, V., Evans, D.S., Germany, G.A., Greer, M.S., Holeman, E., Kadinsky-Cade, K., Rich, F.J., Xu, W., 2008. Seasonal, Kp, solar wind, and solar flux variations in long-term single-pass satellite estimates of electron and ion auroral hemispheric power. J. Geophys. Res. Space Phys. 113 (A6). Q13

Engebretson, M.J., Yeoman, T.K., Oksavik, K., Søraas, F., Sigernes, F., Moen, J.I., Johnsen, M.G., Pilipenko, V.A., Posch, J.L., Lessard, M.R., et al., 2013. Multi-instrument observations from Svalbard of a traveling convection vortex, electromagnetic ion cyclotron wave burst, and proton precipitation associated with a bow shock instability. J. Geophys. Res. Space Phys. 118 (6), 2975–2997.

Engebretson, M.J., Pilipenko, V.A., Ahmed, L.Y., Posch, J.L., Steinmetz, E.S., Moldwin, M.B., Connors, M.G., Weygand, J.M., Mann, I.R., Boteler, D.H., et al., 2019a. Nighttime magnetic perturbation events observed in Arctic Canada: 1. Survey and statistical analysis. J. Geophys. Res. Space Phys. 124 (9), 7442–7458.

Engebretson, M.J., Steinmetz, E.S., Posch, J.L., Pilipenko, V.A., Moldwin, M.B., Connors, M.G., Boteler, D.H., Mann, I.R., Hartinger, M.D., Weygand, J.M., et al., 2019b. Nighttime magnetic perturbation events observed in Arctic Canada: 2. Multiple-instrument observations. J. Geophys. Res. Space Phys. 124 (9), 7459–7476.

Eriksson, A.I., Holback, B., Dovner, P.O., Boström, R., Holmgren, G., André, M., Eliasson, L., Kintner, P. M., 1994. Freja observations of correlated small-scale density depletions and enhanced lower hybrid waves. Geophys. Res. Lett. 21 (17), 1843–1846. https://doi.org/10.1029/94GL00174.

Fang, X., Liemohn, M.W., Kozyra, J.U., Solomon, S.C., 2004. Quantification of the spreading effect of auroral proton precipitation. J. Geophys. Res. Space Phys. 109 (A4). Q14

Fang, X., Liemohn, M.W., Kozyra, J.U., Solomon, S.C., 2005. Study of the proton arc spreading effect on primary ionization rates. J. Geophys. Res. Space Phys. 110 (A7). Q15

Fang, X., Liemohn, M.W., Kozyra, J.U., Evans, D.S., 2007a. Global 30–240 keV proton precipitation in the 17–18 April 2002 geomagnetic storms: 2. Conductances and beam spreading. J. Geophys. Res. Space Phys. 112 (A5). Q16

Fang, X., Liemohn, M.W., Kozyra, J.U., Evans, D.S., DeJong, A.D., Emery, B.A., 2007b. Global 30–240 keV proton precipitation in the 17–18 April 2002 geomagnetic storms: 1. Patterns. J. Geophys. Res. Space Phys. 112 (A5). Q17

Fang, X., Ridley, A.J., Liemohn, M.W., Kozyra, J.U., Evans, D.S., 2007c. Global 30–240 keV proton precipitation in the 17–18 April 2002 geomagnetic storms: 3. Impact on the ionosphere and thermosphere. J. Geophys. Res. Space Phys. 112 (A7). Q18

To protect the rights of the author(s) and publisher we inform you that this PDF is an uncorrected proof for internal business use only by the author(s), editor(s), reviewer(s), Elsevier and typesetter SPi. It is not allowed to publish this proof online or in print. This proof copy is the copyright property of the publisher and is confidential until formal publication.

These proofs may contain colour figures. Those figures may print black and white in the final printed book if a colour print product has not been planned. The colour figures will appear in colour in all electronic versions of this book.

Fang, X., Randall, C.E., Lummerzheim, D., Solomon, S.C., Mills, M.J., Marsh, D.R., Jackman, C.H., Wang, W., Lu, G., 2008. Electron impact ionization: a new parameterization for 100 eV to 1 MeV electrons. J. Geophys. Res. Space Phys. 113 (A9). Q19

Fang, X., Randall, C.E., Lummerzheim, D., Wang, W., Lu, G., Solomon, S.C., Frahm, R.A., 2010. Parameterization of monoenergetic electron impact ionization. Geophys. Res. Lett. 37 (22). Q20

Fang, X., Lummerzheim, D., Jackman, C.H., 2013. Proton impact ionization and a fast calculation method. J. Geophys. Res. Space Phys. 118 (8), 5369–5378.

Farley, D.T., 1963a. A plasma instability resulting in field-aligned irregularities in the ionosphere. J. Geophys. Res. 68, 6083.

Farley, D.T., 1963b. Two-stream plasma instability as a source of irregularities in the ionosphere. Phys. Rev. Lett. 10 (7), 279–282.

Fedorov, E., Pilipenko, V., Engebretson, M.J., 2001. ULF wave damping in the auroral acceleration region. J. Geophys. Res. Space Phys. 106 (A4), 6203–6212.

Foster, J., Erickson, P., 2000. Simultaneous observations of E-region coherent backscatter and electric field amplitude at F-region heights with the Millstone Hill UHF Radar. Geophys. Res. Lett. 27 (19), 3177–3180. https://doi.org/10.1029/2000GL000042.

Foster, J.C., Erickson, P.J., Lind, F.D., Rideout, W., 2004. Millstone Hill coherent-scatter radar observations of electric field variability in the sub-auroral polarization stream. Geophys. Res. Lett. 31 (21), L21803. https://doi.org/10.1029/2004GL021271.

Frahm, R.A., Winningham, J.D., Sharber, J.R., Link, R., Crowley, G., Gaines, E.E., Chenette, D.L., Anderson, B.J., Potemra, T.A., 1997. The diffuse aurora: a significant source of ionization in the middle atmosphere. J. Geophys. Res. Atmos. 102 (D23), 28203–28214.

Friis-Christensen, E., Vennerstrøm, S., Clauer, C.R., McHenry, M.A., 1988. Irregular magnetic pulsations in the polar cleft caused by traveling ionospheric convection vortices. Adv. Space Res. 8 (9–10), 311–314.

Gaisser, T.K., Engel, R., Resconi, E., 2016. Cosmic Rays and Particle Physics. Cambridge University Press. Q21

Galand, M., Lilensten, J., Kofman, W., Sidje, R.B., 1997. Proton transport model in the ionosphere: 1. Multistream approach of the transport equations. J. Geophys. Res. Space Phys. 102 (A10), 22261–22272.

Galand, M., Roble, R.G., Lummerzheim, D., 1999. Ionization by energetic protons in thermosphere-ionosphere electrodynamics general circulation model. J. Geophys. Res. Space Phys. 104 (A12), 27973–27989.

Gérard, J.-C., Hubert, B., Bisikalo, D.V., Shematovich, V.I., 2000. A model of the Lyman-α line profile in the proton aurora. J. Geophys. Res. Space Phys. 105 (A7), 15795–15805.

Glasmeier, K.-H., 1992. Traveling magnetospheric convection twin-vortices-observations and theory. Ann. Geophys. 10 (8), 547–565.

Glasmeier, K.H., et al., 1984. On the influence of ionospheres with non-uniform conductivity distribution on hydromagnetic waves. J. Geophys. 54 (1), 125–137.

Goldberg, R.A., Jackman, C.H., Barcus, J.R., Søraas, F., 1984. Nighttime auroral energy deposition in the middle atmosphere. J. Geophys. Res. Space Phys. 89 (A7), 5581–5596.

Green, A.E.S., Jackman, C.H., Garvey, R.H., 1977. Electron impact on atmospheric gases, 2. Yield spectra. J. Geophys. Res. 82 (32), 5104–5111.

Gurevich, A.V., 1978. Nonlinear Phenomena in the Ionosphere. Springer, New York, https://doi.org/10.1007/978-3-642-87649-3.

Haldoupis, C., Schlegel, K., Farley, D.T., 1996. An explanation for type 1 radar echoes from the midlatitude E-region ionosphere. Geophys. Res. Lett. 23 (1), 97–100. https://doi.org/10.1029/95GL03585.

Haraguchi, K., Kawano, H., Yumoto, K., Ohtani, S., Higuchi, T., Ueno, G., 2004. Ionospheric conductivity dependence of dayside region-0, 1, and 2 field-aligned current systems: statistical study with DMSP-F7. Ann. Geophys. 22 (8), 2775–2783.

Hardy, D.A., Gussenhoven, M.S., Raistrick, R., McNeil, W.J., 1987. Statistical and functional representations of the pattern of auroral energy flux, number flux, and conductivity. J. Geophys. Res. Space Phys. 92 (A11), 12275–12294.

Hardy, D.A., Gussenhoven, M.S., Brautigam, D., 1989. A statistical model of auroral ion precipitation. J. Geophys. Res. Space Phys. 94 (A1), 370–392.

To protect the rights of the author(s) and publisher we inform you that this PDF is an uncorrected proof for internal business use only by the author(s), editor(s), reviewer(s), Elsevier and typesetter SPi. It is not allowed to publish this proof online or in print. This proof copy is the copyright property of the publisher and is confidential until formal publication.

These proofs may contain colour figures. Those figures may print black and white in the final printed book if a colour print product has not been planned. The colour figures will appear in colour in all electronic versions of this book.

Hartinger, M.D., Xu, Z., Clauer, C.R., Yu, Y., Weimer, D.R., Kim, H., Pilipenko, V., Welling, D.T., Behlke, R., Willer, A.N., 2017. Associating ground magnetometer observations with current or voltage generators. J. Geophys. Res. Space Phys. 122 (7), 7130–7141.

Hedin, A.E., 1991. Extension of the MSIS thermosphere model into the middle and lower atmosphere. J. Geophys. Res. Space Phys. 96 (A2), 1159–1172.

Hill, T.L., 1956. Statistical Mechanics: Principles and Selected Applications. Dover Books on Physics, McGraw-Hill, ISBN: 9780486653907.

Hoh, F.C., 1963. Instability of penning-type discharges. Phys. Fluids 6, 1184–1191. https://doi.org/10.1063/1.1706878.

Hollweg, J.V., 1999. Kinetic Alfvén wave revisited. J. Geophys. Res. 104 (A7), 14811–14820. https://doi.org/10.1029/1998JA900132.

Huang, K., 1963. Statistical Mechanics. Wiley. ISBN 9780471417602.

Hughes, W.J., Southwood, D.J., 1976. The screening of micropulsation signals by the atmosphere and ionosphere. J. Geophys. Res. 81 (19), 3234–3240.

Jackman, C.H., Frederick, J.E., Stolarski, R.S., 1980. Production of odd nitrogen in the stratosphere and mesosphere: an intercomparison of source strengths. J. Geophys. Res. Oceans 85 (C12), 7495–7505.

Jackman, C.H., Marsh, D.R., Vitt, F.M., Garcia, R.R., Fleming, E.L., Labow, G.J., Randall, C.E., López-Puertas, M., Funke, B., von Clarmann, T., et al., 2008. Short- and medium-term atmospheric constituent effects of very large solar proton events. Atmos. Chem. Phys. 8 (3), 765–785.

Jasperse, J.R., 1997. Transport theoretic solutions for the beam-spreading effect in the proton-hydrogen aurora. Geophys. Res. Lett. 24 (11), 1415–1418.

Jasperse, J.R., Basu, B., 1982. Transport theoretic solutions for auroral proton and H atom fluxes and related quantities. J. Geophys. Res. Space Phys. 87 (A2), 811–822.

Kagan, L.M., Kelley, M.C., 2000. A thermal mechanism for generation of small-scale irregularities in the ionospheric E region. J. Geophys. Res. 105, 5291–5302. https://doi.org/10.1029/1999JA900415.

Kelley, M.C., 2009. The Earth's Ionosphere: Plasma Physics and Electrodynamics. Academic Press. Q22

Khazanov, G.V., 2011. Kinetic Theory of the Inner Magnetospheric Plasma. Springer, New York, https://doi.org/10.1007/978-1-4419-6797-8.

Khazanov, G.V., Liemohn, M.W., Newman, T.S., Fok, M.C., Spiro, R.W., 2003. Self-consistent magnetosphere-ionosphere coupling: theoretical studies. J. Geophys. Res. Space Phys. 108 (A3), 1122. https://doi.org/10.1029/2002JA009624.

Khazanov, G.V., Khabibrakhmanov, I.K., Glocer, A., 2012. Kinetic description of ionospheric outflows based on the exact form of Fokker-Planck collision operator: electrons. J. Geophys. Res. Space Phys. 117 (A11), A11203. https://doi.org/10.1029/2012JA018082.

Khazanov, G.V., Glocer, A., Himwich, E.W., 2014. Magnetosphere-ionosphere energy interchange in the electron diffuse aurora. J. Geophys. Res. Space Phys. 119 (1), 171–184. https://doi.org/10.1002/2013JA019325.

Kim, H., Cai, X., Clauer, C.R., Kunduri, B.S.R., Matzka, J., Stolle, C., Weimer, D.R., 2013. Geomagnetic response to solar wind dynamic pressure impulse events at high-latitude conjugate points. J. Geophys. Res. Space Phys. 118 (10), 6055–6071.

Kim, H., Clauer, C.R., Engebretson, M.J., Matzka, J., Sibeck, D.G., Singer, H.J., Stolle, C., Weimer, D.R., Xu, Z., 2015. Conjugate observations of traveling convection vortices associated with transient events at the magnetopause. J. Geophys. Res. Space Phys. 120 (3), 2015–2035.

Kintner, P.M., Vago, J., Chesney, S., Arnoldy, R.L., Lynch, K.A., Pollock, C.J., Moore, T.E., 1992. Localized lower hybrid acceleration of ionospheric plasma. Phys. Rev. Lett. 68 (16), 2448–2451. https://doi.org/10.1103/PhysRevLett.68.2448.

Kintner, P.M., Bonnell, J., Arnoldy, R., Lynch, K., Pollock, C., Moore, T., 1996. SCIFER-transverse ion acceleration and plasma waves. Geophys. Res. Lett. 23 (14), 1873–1876. https://doi.org/10.1029/96GL01863.

Kivelson, M.G., Southwood, D.J., 1986. Coupling of global magnetospheric MHD eigenmodes to field line resonances. J. Geophys. Res. Space Phys. 91 (A4), 4345–4351.

Kozelov, B.V., 1993. Influence of the dipolar magnetic field on transport of proton-H atom fluxes in the atmosphere. Ann. Geophys. 11 (8), 697–704.

To protect the rights of the author(s) and publisher we inform you that this PDF is an uncorrected proof for internal business use only by the author(s), editor(s), reviewer(s), Elsevier and typesetter SPi. It is not allowed to publish this proof online or in print. This proof copy is the copyright property of the publisher and is confidential until formal publication.

These proofs may contain colour figures. Those figures may print black and white in the final printed book if a colour print product has not been planned. The colour figures will appear in colour in all electronic versions of this book.

Kuby, M.J., Roberts, T.D., Upchurch, C.D., Tierney, S., 2009. Network analysis. In: Rob, K., Nigel, T. (Eds.), International Encyclopedia of Human Geography. Elsevier, Oxford, pp. 391–398.

Kudeki, E., Fejer, B.G., Farley, D.T., Hanuise, C., 1987. The Condor equatorial electrojet campaign-radar results. J. Geophys. Res. 92, 13561–13577. https://doi.org/10.1029/JA092iA12p13561.

Lam, M.M., Rodger, A.S., 2004. A test of the magnetospheric source of traveling convection vortices. J. Geophys. Res. Space Phys. 109 (A2). Q23

Lanzerotti, L.J., Wolfe, A., Trivedi, N., Maclennan, C.G., Medford, L.V., 1990. Magnetic impulse events at high latitudes: magnetopause and boundary layer plasma processes. J. Geophys. Res. Space Phys. 95 (A1), 97–107.

Lanzerotti, L.J., Konik, R.M., Wolfe, A., Venkatesan, D., Maclennan, C.G., 1991. Cusp latitude magnetic impulse events: 1. Occurrence statistics. J. Geophys. Res. Space Phys. 96 (A8), 14009–14022.

Lazarev, V.I., 1967. Absorption of the energy of an electron beam in the upper atmosphere. Geomagn. Aeron. 7, 219.

Lehtinen, N.G., Bell, T.F., Inan, U.S., 1999. Monte Carlo simulation of runaway MeV electron breakdown with application to red sprites and terrestrial gamma ray flashes. J. Geophys. Res. Space Phys. 104 (A11), 24699–24712.

Link, R., 1992. Feautrier solution of the electron transport equation. J. Geophys. Res. Space Phys. 97 (A1), 159–169.

Liou, K., Sotirelis, T., Mitchell, E.J., 2018. North-South asymmetry in the geographic location of auroral substorms correlated with ionospheric effects. Sci. Rep. 8 (1), 1–6.

Livadiotis, G., McComas, D.J., 2009. Beyond kappa distributions: exploiting Tsallis statistical mechanics in space plasmas. J. Geophys. Res. Space Phys. 114 (A11), A11105. https://doi.org/10.1029/2009JA014352.

Longley, W.J., Oppenheim, M.M., Pedatella, N.M., Dimant, Y.S., 2020. The photoelectron-driven upper hybrid instability as the cause of 150-km echoes. Geophys. Res. Lett. 47 (8). https://doi.org/10.1029/2020GL087391. e2020GL087391.

Lorentzen, D.A., 2000. Latitudinal and longitudinal dispersion of energetic auroral protons. Ann. Geophys. 18 (1), 81–89.

Lummerzheim, D., 1992. Comparison of Energy Dissipation Functions for High Energy Auroral Electron and Ion Precipitation. Geophysical Institute, University of Alaska Fairbanks. Q24

Lummerzheim, D., Lilensten, J., 1994. Electron transport and energy degradation in the ionosphere: evaluation of the numerical solution, comparison with laboratory experiments and auroral observations. Ann. Geophys. 12 (10), 1039–1051.

Lummerzheim, D., Rees, M.H., Anderson, H.R., 1989. Angular dependent transport of auroral electrons in the upper atmosphere. Planet. Space Sci. 37 (1), 109–129.

Lyons, L.R., 1997. Magnetospheric processes leading to precipitation. In: Transport Across the Boundaries of the Magnetosphere, Springer, pp. 109–132. Q25

Lysak, R.L., 1985. Auroral electrodynamics with current and voltage generators. J. Geophys. Res. Space Phys. 90 (A5), 4178–4190.

Lysak, R.L., 1990. Electrodynamic coupling of the magnetosphere and ionosphere. Space Sci. Rev. 52 (1), 33–87.

Lysak, R.L., Lotko, W., 1996. On the kinetic dispersion relation for shear Alfvén waves. J. Geophys. Res. 101 (A3), 5085–5094. https://doi.org/10.1029/95JA03712.

Maeda, K., Tsuda, T., Maeda, H., 1963. Theoretical interpretation of the equatorial sporadic *E* layers. Phys. Rev. Lett. 11 (9), 406–407. https://doi.org/10.1103/PhysRevLett.11.406.

McHenry, M.A., Clauer, C.R., 1987. Modeled ground magnetic signatures of flux transfer events. J. Geophys. Res. Space Phys. 92 (A10), 11231–11240.

Mesick, K.E., Feldman, W.C., Coupland, D.D.S., Stonehill, L.C., 2018. Benchmarking Geant4 for simulating galactic cosmic ray interactions within planetary bodies. Earth Space Sci. 5 (7), 324–338.

Mewaldt, R.A., Mason, G.M., Gloeckler, G., Christian, E.R., Cohen, C.M.S., Cummings, A.C., Davis, A. J., Dwyer, J.R., Gold, R.E., Krimigis, S.M., Leske, R.A., Mazur, J.E., Stone, E.C., von Rosenvinge, T. T., Wiedenbeck, M.E., Zurbuchen, T.H., 2001. Long-term fluences of energetic particles in the heliosphere. In: Wimmer-Schweingruber, R.F. (Ed.), American Institute of Physics Conference Series. Joint SOHO/ACE Workshop "Solar and Galactic Composition", November, vol. 598, pp. 165–170.

To protect the rights of the author(s) and publisher we inform you that this PDF is an uncorrected proof for internal business use only by the author(s), editor(s), reviewer(s), Elsevier and typesetter SPi. It is not allowed to publish this proof online or in print. This proof copy is the copyright property of the publisher and is confidential until formal publication.

These proofs may contain colour figures. Those figures may print black and white in the final printed book if a colour print product has not been planned. The colour figures will appear in colour in all electronic versions of this book.

Moore, T.E., Lundin, R., Alcayde, D., André, M., Ganguli, S.B., Temerin, M., Yau, A., 1999. Chapter 2—Source processes in the high-latitude ionosphere. Space Sci. Rev. 88, 7–84. https://doi.org/10.1023/A:1005299616446.

Moretto, T., Yahnin, A., 1998. Mapping travelling convection vortex events with respect to energetic particle boundaries. Ann. Geophys. 16 (8), 891–899.

Murr, D.L., Hughes, W.J., 2003. Solar wind drivers of traveling convection vortices. Geophys. Res. Lett. 30 (7). Q26

Murr, D.L., Hughes, W.J., Rodger, A.S., Zesta, E., Frey, H.U., Weatherwax, A.T., 2002. Conjugate observations of traveling convection vortices: the field-aligned current system. J. Geophys. Res. Space Phys. 107 (A10), SIA-14.

Nagy, A.F., Banks, P.M., 1970. Photoelectron fluxes in the ionosphere. J. Geophys. Res. 75 (31), 6260–6270.

Newell, P.T., Meng, C.I., Lyons, K.M., 1996. Discrete aurorae are suppressed in sunlight. Nature 381 (6585), 766–767.

Newell, P.T., Sotirelis, T., Wing, S., 2009. Diffuse, monoenergetic, and broadband aurora: the global precipitation budget. J. Geophys. Res. Space Phys. 114 (A9), A09207. https://doi.org/10.1029/2009JA014326.

Newton, R.S., Southwood, D.J., Hughes, W.J., 1978. Damping of geomagnetic pulsations by the ionosphere. Planet. Space Sci. 26 (3), 201–209.

Ni, B., Thorne, R.M., Horne, R.B., Meredith, N.P., Shprits, Y.Y., Chen, L., Li, W., 2011a. Resonant scattering of plasma sheet electrons leading to diffuse auroral precipitation: 1. Evaluation for electrostatic electron cyclotron harmonic waves. J. Geophys. Res. Space Phys. 116 (A4). https://doi.org/10.1029/2010JA016232.

Ni, B., Thorne, R.M., Meredith, N.P., Horne, R.B., Shprits, Y.Y., 2011b. Resonant scattering of plasma sheet electrons leading to diffuse auroral precipitation: 2. Evaluation for whistler mode chorus waves. J. Geophys. Res. Space Phys. 116 (A4). https://doi.org/10.1029/2010JA016233.

Ni, B., Liang, J., Thorne, R.M., Angelopoulos, V., Horne, R.B., Kubyshkina, M., Spanswick, E., Donovan, E.F., Lummerzheim, D., 2012. Efficient diffuse auroral electron scattering by electrostatic electron cyclotron harmonic waves in the outer magnetosphere: a detailed case study. J. Geophys. Res. Space Phys. 117 (A1), A01218. https://doi.org/10.1029/2011JA017095.

Nicholson, D.R., 1983. Introduction to Plasma Theory. Wiley, New York.

Obana, Y., Yoshikawa, A., Olson, J.V., Morris, R.J., Fraser, B.J., Yumoto, K., 2005. North-South asymmetry of the amplitude of high-latitude Pc 3–5 pulsations: observations at conjugate stations. J. Geophys. Res. Space Phys. 110 (A10).

Oppenheim, M.M., Dimant, Y.S., 2013. Kinetic simulations of 3-D Farley-Buneman turbulence and anomalous electron heating. J. Geophys. Res. Space Phys. 118, 1306–1318. https://doi.org/10.1002/jgra.50196.

Pelowitz, D.B., et al., 2005. MCNPX User's Manual Version 2.5. 0. Los Alamos Natl. Lab. 76, 473.

Pfaff, R.F., Kelley, M.C., Kudeki, E., Fejer, B.G., Baker, K.D., 1987a. Electric field and plasma density measurements in the strongly driven daytime equatorial electrojet. 1. The unstable layer and gradient drift waves. J. Geophys. Res. 92, 13578–13596. https://doi.org/10.1029/JA092iA12p13578.

Pfaff, R.F., Kelley, M.C., Kudeki, E., Fejer, B.G., Baker, K.D., 1987b. Electric field and plasma density measurements in the strongly driven daytime equatorial electrojet. 2. Two-stream waves. J. Geophys. Res. 92, 13597–13612. https://doi.org/10.1029/JA092iA12p13597.

Pierrard, V., Lazar, M., 2010. Kappa distributions: theory and applications in space plasmas. Solar Phys. 267, 153–174. https://doi.org/10.1007/s11207-010-9640-2.

Pilipenko, V., Fedorov, E., Heilig, B., Engebretson, M.J., Sutcliffe, P., Lühr, H., 2011. ULF waves in the topside ionosphere: satellite observations and modeling. In: The Dynamic Magnetosphere, Springer, pp. 257–269. Q27

Pilipenko, V.A., Fedorov, E.N., Hartinger, M.D., Engebretson, M.J., 2019. Electromagnetic fields of magnetospheric ULF disturbances in the ionosphere: current/voltage dichotomy. J. Geophys. Res. Space Phys. 124 (1), 109–121.

To protect the rights of the author(s) and publisher we inform you that this PDF is an uncorrected proof for internal business use only by the author(s), editor(s), reviewer(s), Elsevier and typesetter SPi. It is not allowed to publish this proof online or in print. This proof copy is the copyright property of the publisher and is confidential until formal publication.

These proofs may contain colour figures. Those figures may print black and white in the final printed book if a colour print product has not been planned. The colour figures will appear in colour in all electronic versions of this book.

Pilipenko, V.A., Martines-Bedenko, V.A., Coyle, S., Fedorov, E.N., Hartinger, M.D., Engebretson, M.J., Edwards, T.R., 2021. Conjugate properties of magnetospheric Pc5 waves: Antarctica-Greenland comparison. J. Geophys. Res. Space Phys. e2020JA028048. Q28

Porter, H.S., Green, A.E.S., 1975. Comparison of Monte Carlo and continuous slowing-down approximation treatments of 1-keV proton energy deposition in N2. J. Appl. Phys. 46 (11), 5030–5038.

Porter, H.S., Jackman, C.H., Green, A.E.S., 1976. Efficiencies for production of atomic nitrogen and oxygen by relativistic proton impact in air. J. Chem. Phys. 65 (1), 154–167.

Reames, D.V., 1999. Particle acceleration at the Sun and in the heliosphere. Space Sci. Rev. 90 (3), 413–491.

Rees, M.H., 1963. Auroral ionization and excitation by incident energetic electrons. Planet. Space Sci. 11 (10), 1209–1218.

Rees, M.H., 1964. Ionization in the Earth's atmosphere by aurorally associated bremsstrahlung X-rays. Planet. Space Sci. 12 (11), 1093–1108.

Rees, M.H., 1969. Auroral electrons. Space Sci. Rev. 10 (3), 413–441.

Reid, G.C., 1961. A study of the enhanced ionization produced by solar protons during a polar cap absorption event. J. Geophys. Res. 66 (12), 4071–4085.

Ridley, A.J., Gombosi, T.I., DeZeeuw, D.L., 2004. Ionospheric control of the magnetosphere: conductance. Ann. Geophys. 22 (2), 567–584.

Robinson, R.M., Vondrak, R.R., Miller, K., Dabbs, T., Hardy, D., 1987. On calculating ionospheric conductances from the flux and energy of precipitating electrons. J. Geophys. Res. Space Phys. 92 (A3), 2565–2569.

Roble, R.G., Ridley, E.C., 1987. An auroral model for the NCAR thermospheric general circulation model (TGCM). Ann. Geophys. 5, 369–382.

Roeder, J.L., Koons, H.C., 1989. A survey of electron cyclotron waves in the magnetosphere and the diffuse auroral electron precipitation. J. Geophys. Res. Space Phys. 94 (A3), 2529–2541. https://doi.org/10.1029/JA094iA03p02529.

Rosenberg, T.J., Siren, J.C., Lanzerotti, L.J., 1980. High time resolution riometer and X-ray measurements of conjugate electron precipitation from the magnetosphere. Nature 283 (5744), 278–280.

Schmidt, M.J., Gary, S.P., 1973. Density gradients and the Farley-Buneman instability. J. Geophys. Res. 78, 8261–8265. https://doi.org/10.1029/JA078i034p08261.

Scholz, C.H., 2007. 6.10-Fault mechanics. In: Gerald, S. (Ed.), Treatise on Geophysics. Elsevier, Amsterdam, pp. 441–483.

Schroeder, J.W.R., Skiff, F., Howes, G.G., Kletzing, C.A., Carter, T.A., Dorfman, S., 2017. Linear theory and measurements of electron oscillations in an inertial Alfvén wave. Phys. Plasmas 24 (3), 032902. https://doi.org/10.1063/1.4978293.

Schröter, J., Heber, B., Steinhilber, F., Kallenrode, M.B., 2006. Energetic particles in the atmosphere: a Monte-Carlo simulation. Adv. Space Res. 37 (8), 1597–1601.

Schunk, R.W., Nagy, A.F., 2004. Ionospheres. Cambridge University Press, p. 570. Q29

Schunk, R., Nagy, A., 2009. Ionospheres: Physics, Plasma Physics, and Chemistry. Cambridge University Press. Q30

Schwadron, N.A., Dayeh, M.A., Desai, M., Fahr, H., Jokipii, J.R., Lee, M.A., 2010. Superposition of Stochastic Processes and the Resulting Particle Distributions. Astrophys. J. 713, 1386–1392. https://doi.org/10.1088/0004-637X/713/2/1386.

Shalimov, S., Haldoupis, C., 2005. E-region wind-driven electrical coupling of patchy sporadic-E and spread-F at midlatitude. Ann. Geophys. 23 (6), 2095–2105. https://doi.org/10.5194/angeo-23-2095-2005.

Sharp, R.D., Johnson, R.G., Shelley, E.G., 1977. Observation of an ionospheric acceleration mechanism producing energetic (keV) ions primarily normal to the geomagnetic field direction. J. Geophys. Res. 82 (22), 3324. https://doi.org/10.1029/JA082i022p03324.

Shelley, E.G., Sharp, R.D., Johnson, R.G., 1976. Satellite observations of an ionospheric acceleration mechanism. Geophys. Res. Lett. 3 (11), 654–656. https://doi.org/10.1029/GL003i011p00654.

Shi, J.K., Cheng, Z.W., Zhang, T.L., Dunlop, M., Liu, Z.X., Torkar, K., Fazakerley, A., Lucek, E., Rème, H., Dandouras, I., et al., 2010. South-North asymmetry of field-aligned currents in the magnetotail observed by Cluster. J. Geophys. Res. Space Phys. 115 (A7).

To protect the rights of the author(s) and publisher we inform you that this PDF is an uncorrected proof for internal business use only by the author(s), editor(s), reviewer(s), Elsevier and typesetter SPi. It is not allowed to publish this proof online or in print. This proof copy is the copyright property of the publisher and is confidential until formal publication.

These proofs may contain colour figures. Those figures may print black and white in the final printed book if a colour print product has not been planned. The colour figures will appear in colour in all electronic versions of this book.

Shinbori, A., Tsuji, Y., Kikuchi, T., Araki, T., Ikeda, A., Uozumi, T., Baishev, D., Shevtsov, B.M., Nagatsuma, T., Yumoto, K., 2012. Magnetic local time and latitude dependence of amplitude of the main impulse (MI) of geomagnetic sudden commencements and its seasonal variation. J. Geophys. Res. Space Phys. 117 (A8). Q31

Shkarofsky, I.P., Johnston, T.W., Bachynski, M.P., 1966. The Particle Kinetics of Plasmas. Addison-Wesley, Reading, MA.

Sibeck, D.G., Greenwald, R.A., Bristow, W.A., Korotova, G.I., 1996. Concerning possible effects of ionospheric conductivity upon the occurrence patterns of impulsive events in high-latitude ground magnetograms. J. Geophys. Res. Space Phys. 101 (A6), 13407–13412.

Simon, A., 1963. Instability of a partially ionized plasma in crossed electric and magnetic fields. Phys. Fluids 6, 382–388. https://doi.org/10.1063/1.1706743.

Smart, D.F., Shea, M.A., Flückiger, E.O., 2000. Magnetospheric models and trajectory computations. Cosmic Rays Earth, 305–333. Q32

Solomon, S.C., 1993. Auroral electron transport using the Monte Carlo method. Geophys. Res. Lett. 20 (3), 185–188.

Solomon, S.C., 2001. Auroral particle transport using Monte Carlo and hybrid methods. J. Geophys. Res. Space Phys. 106 (A1), 107–116.

Solomon, S.C., Abreu, V.J., 1989. The 630 nm dayglow. J. Geophys. Res. Space Phys. 94 (A6), 6817–6824.

Solomon, S.C., Hays, P.B., Abreu, V.J., 1988. The auroral 6300 Å emission: observations and modeling. J. Geophys. Res. Space Phys. 93 (A9), 9867–9882.

Spanswick, E., Donovan, E., Baker, G., 2005. Pc5 modulation of high energy electron precipitation: particle interaction regions and scattering efficiency. Ann. Geophys. 23 (5), 1533–1542.

Spencer, L.V.C., 1959. Energy Dissipation by Fast Electrons. vol. 1 US Department of Commerce, National Bureau of Standards. Q33

St.-Maurice, J.P., Schlegel, K., Banks, P.M., 1981. Anomalous heating of the polar E region by unstable plasma waves. II—theory. J. Geophys. Res. 86, 1453–1462. https://doi.org/10.1029/JA086iA03p01453.

Stasiewicz, K., Bellan, P., Chaston, C., Kletzing, C., Lysak, R., Maggs, J., Pokhotelov, O., Seyler, C., Shukla, P., Stenflo, L., Streltsov, A., Wahlund, J.E., 2000. Small scale Alfvénic structure in the aurora. Space Sci. Rev. 92, 423–533.

Strickland, D.J., Book, D.L., Coffey, T.P., Fedder, J.A., 1976. Transport equation techniques for the deposition of auroral electrons. J. Geophys. Res. 81 (16), 2755–2764.

Strickland, D.J., Daniell Jr, R.E., Jasperse, J.R., Basu, B., 1993. Transport-theoretic model for the electron-proton-hydrogen atom aurora: 2. Model results. J. Geophys. Res. Space Phys. 98 (A12), 21533–21548.

Struchtrup, H., 1997. The BGK-model with velocity-dependent collision frequency. Contin. Mech. Thermodyn. 9 (1), 23–31. https://doi.org/10.1007/s001610050053.

Sutcliffe, P.R., Rostoker, G., 1979. Dependence of Pc5 micropulsation power on conductivity variations in the morning sector. Planet. Space Sci. 27 (5), 631–642.

Synnes, S.A., Søraas, F., Hansen, J.P., 1998. Monte-Carlo simulations of proton aurora. J. Atmos. Sol.-Terr. Phys. 60 (17), 1695–1705.

ter Haar, D., 1954. Elements of Statistical Mechanics. Rinehart. Q34

Thorne, R.M., Ni, B., Tao, X., Horne, R.B., Meredith, N.P., 2010. Scattering by chorus waves as the dominant cause of diffuse auroral precipitation. Nature 467 (7318), 943–946. https://doi.org/10.1038/nature09467.

Usoskin, I.G., Kovaltsov, G.A., 2006. Cosmic ray induced ionization in the atmosphere: full modeling and practical applications. J. Geophys. Res. Atmos. 111 (D21).

Vasyliunas, V.M., 1968. A survey of low-energy electrons in the evening sector of the magnetosphere with OGO 1 and OGO 3. J. Geophys. Res. 73, 2839–2884. https://doi.org/10.1029/JA073i009p02839.

Vorob'ev, V.G., 1993. Dynamics of Hall vortices in a day-time high-latitude region. Geomagn. Aeron. 33 (5), 58–68.

Wahlund, J.E., Opgenoorth, H.J., Haggstrom, I., Winser, K.J., Jones, G.O.L., 1992. EISCAT observations of topside ionospheric ion outflows during auroral activity: revisited. J. Geophys. Res. (A3), 3019–3037. https://doi.org/10.1029/91JA02438.

To protect the rights of the author(s) and publisher we inform you that this PDF is an uncorrected proof for internal business use only by the author(s), editor(s), reviewer(s), Elsevier and typesetter SPi. It is not allowed to publish this proof online or in print. This proof copy is the copyright property of the publisher and is confidential until formal publication.

These proofs may contain colour figures. Those figures may print black and white in the final printed book if a colour print product has not been planned. The colour figures will appear in colour in all electronic versions of this book.

Watanabe, T.H., 2014. A unified model of auroral arc growth and electron acceleration in the magnetosphere-ionosphere coupling. Geophys. Res. Lett. 41 (17), 6071–6077. https://doi.org/10.1002/2014GL061166.

Wedlund, C.S., Gronoff, G., Lilensten, J., Ménager, H., Barthélemy, M., 2011. Comprehensive calculation of the energy per ion pair or w values for five major planetary upper atmospheres. Ann. Geophys. 29 (1), 187–195.

Welling, D.T., André, M., Dandouras, I., Delcourt, D., Fazakerley, A., Fontaine, D., Foster, J., Ilie, R., Kistler, L., Lee, J.H., Liemohn, M.W., Slavin, J.A., Wang, C.-P., Wiltberger, M., Yau, A., 2015. The Earth: plasma sources, losses, and transport processes. Space Sci. Rev. 192 (1–4), 145–208. https://doi.org/10.1007/s11214-015-0187-2.

Werner, C.J., et al., 2017. MCNP User's Manual-Code Version 6.2. Los Alamos National Laboratory, LA-UR-17-29981.

Wiltberger, M., Merkin, V., Zhang, B., Toffoletto, F., Oppenheim, M., Wang, W., Lyon, J.G., Liu, J., Dimant, Y., Sitnov, M.I., Stephens, G.K., 2017. Effects of electrojet turbulence on a magnetosphere-ionosphere simulation of a geomagnetic storm. J. Geophys. Res. Space Phys. 122 (5), 5008–5027. https://doi.org/10.1002/2016JA023700.

Wissing, J.M., Kallenrode, M.B., 2009. Atmospheric ionization module Osnabrück (AIMOS): a 3-D model to determine atmospheric ionization by energetic charged particles from different populations. J. Geophys. Res. Space Phys. 114 (A6).

Wolf, R.A., 1970. Effects of ionospheric conductivity on convective flow of plasma in the magnetosphere. J. Geophys. Res. 75 (25), 4677–4698.

Wygant, J.R., Keiling, A., Cattell, C.A., Lysak, R.L., Temerin, M., Mozer, F.S., Kletzing, C.A., Scudder, J.D., Streltsov, V., Lotko, W., Russell, C.T., 2002. Evidence for kinetic Alfvén waves and parallel electron energization at 4–6 R_E altitudes in the plasma sheet boundary layer. J. Geophys. Res. Space Phys. 107 (A8), 1201. https://doi.org/10.1029/2001JA900113.

Xu, W., Marshall, R.A., Fang, X., Turunen, E., Kero, A., 2018. On the effects of bremsstrahlung radiation during energetic electron precipitation. Geophys. Res. Lett. 45 (2), 1167–1176.

Yamauchi, M., 2019. Terrestrial ion escape and relevant circulation in space. Ann. Geophys. 37 (6), 1197–1222. https://doi.org/10.5194/angeo-37-1197-2019.

Yau, A.W., André, M., 1997. Sources of ion outflow in the high latitude ionosphere. Space Sci. Rev. 80, 1–25. https://doi.org/10.1023/A:1004947203046.

Young, M.A., Oppenheim, M.M., Dimant, Y.S., 2019. Simulations of secondary Farley-Buneman instability driven by a kilometer-scale primary wave: anomalous transport and formation of flat-topped electric fields. J. Geophys. Res. Space Phys. 124, 734–748. https://doi.org/10.1029/2018JA026072.

Yumoto, K., Pilipenko, V., Fedorov, E., Kurneva, N., Shiokawa, K., 1995. The mechanisms of damping of geomagnetic pulsations. J. Geomagn. Geoelectr. 47 (2), 163–176.

Yumoto, K., Matsuoka, H., Osaki, H., Shiokawa, K., Tanaka, Y., Kitamura, T.I., Tachihara, H., Shinohara, M., Solovyev, S.I., Makarov, G.A., et al., 1996. North/south asymmetry of SC/SI magnetic variations observed along the 210° magnetic meridian. J. Geomagn. Geoelectr. 48 (11), 1333–1340.

Zakharenkova, I., Cherniak, I., 2020. When plasma streams tie up equatorial plasma irregularities with auroral ones. Space Weather 18 (2), e02375. https://doi.org/10.1029/2019SW002375.

Zesta, E., Boudouridis, A., Weygand, J.M., Yizengaw, E., Moldwin, M.B., Chi, P., 2016. Interhemispheric asymmetries in magnetospheric energy input. In: Ionospheric Space Weather: Longitude Dependence and Lower Atmosphere Forcing, Geophysical Monograph Series, 220, pp. 1–20.

To protect the rights of the author(s) and publisher we inform you that this PDF is an uncorrected proof for internal business use only by the author(s), editor(s), reviewer(s), Elsevier and typesetter SPi. It is not allowed to publish this proof online or in print. This proof copy is the copyright property of the publisher and is confidential until formal publication.